Catarina Cerqueira da Silva Simões

Licenciatura em Ciências da Engenharia Química e Bioquímica

Bipolar Membrane Based Energy Storage System: The Acid Base Flow Battery

Dissertação para obtenção do Grau de Mestre em
Engenharia Química e Bioquímica

Orientador: Dr. Svetlozar Velizarov, Investigador Auxiliar, LAQV, Faculdade de Ciências e Tecnologia da Universidade Nova de Lisboa

Co-orientadores: Dr. Michel Saakes, Theme Coordinator, Wetsus

Dr. Michele Tedesco, Theme Coordinator, Wetsus

Júri:

Presidente: Dr. Mário Fernando José Eusébio, Faculdade de Ciências e Tecnologia da Universidade Nova de Lisboa

Arguente: Dr. Vítor Manuel Geraldes Fernandes, Instituto Superior Técnico da Universidade de Lisboa

Membro: Dr. Svetlozar Velizarov, LAQV, Faculdade de Ciências e Tecnologia da Universidade Nova de Lisboa.

FACULDADE DE CIÊNCIAS E TECNOLOGIA
UNIVERSIDADE NOVA DE LISBOA

Setembro, 2018

Catarina Cerqueira da Silva Simões

Licenciatura em Ciências da Engenharia Química e Bioquímica

Bipolar Membrane Based Energy Storage System: The Acid Base Flow Battery

Dissertação para obtenção do Grau de Mestre em
Engenharia Química e Bioquímica

Orientador: Dr. Svetlozar Velizarov, Investigador Auxiliar, LAQV, Faculdade de Ciências e Tecnologia da Universidade Nova de Lisboa

Co-orientadores: Dr. Michel Saakes, Theme Coordinator, Wetsus

Dr. Michele Tedesco, Theme Coordinator, Wetsus

Júri:

Presidente: Dr. Mário Fernando José Eusébio, Faculdade de Ciências e Tecnologia da Universidade Nova de Lisboa

Arguente: Dr. Vítor Manuel Geraldes Fernandes, Instituto Superior Técnico da Universidade de Lisboa

Membro: Dr. Svetlozar Velizarov, LAQV, Faculdade de Ciências e Tecnologia da Universidade Nova de Lisboa

Setembro, 2018

Bipolar Membrane Based Energy Storage System: The Acid Base Flow Battery

Acknowledgements

I would like to express my gratitude to Professor Svetlozar Velizarov and to Michele Tedesco for creating a partnership between FCT-UNL and Wetsus, which gave me opportunity to enrol on a challenging and innovative project. I would also like to thank to Michel Saakes, who welcomed me under his supervision at Wetsus, for his guidance and all the brainstorming we shared. To all the mentioned above, I would like to thank for the motivation and teaching moments given, it was crucial for my success and future!

I would like to thank to everybody at Wetsus that make me feel welcome and confident to finish my master thesis. Also, to all my colleagues and friends who supported me with the decision of going abroad to do this project.

A special thank you:

To my Portuguese family abroad, Mariana, Vanessa and Emanuel, without you I wouldn't had been the same, with our funny Portuguese conversations and travels and everything.

To my international family, Ragne, Francisca, Magali, Ben, Geert-Jan and Advait, thank you for all the crazy moments we had, from travelling and afternoons in the park to football. Your support was amazing in all steps.

To my co-workers of the acid base flow battery, Emad and Bart, together we had interesting discussions and helped each other towards better results.

To my lunch companions, Wokke and Hector, eating tasty food is always inspiring to work better.

To my housemate, Gijs, thank you for the patience, the encouragement and helpful advices in and out the lab.

To my project partners, João, Nuno and Pedro, that helped me in the kick off while we still had project to finish.

To my friends in Portugal that came to visit me, Cláudia, Alexandra and Kostadin, and the ones that couldn't visit, Nuno, Francisco and Nelson, but all supported this adventure and always kept in touch.

Lastly, a big thank you to my family, my parents, my brother and my grandparents, that have been supporting me since the beginning and made this possible.

Abstract

The rapid growth of renewable energy sources creates the necessity of developing efficient electrical energy storage (EES) systems, to assure reliability of the electricity grid. Currently available technologies still either have geographical restrictions, safety issues or environmental problems. In this thesis, the acid base flow battery (AB-FB) is studied. The AB-FB consists of a sustainable flow battery using NaCl as solution and ion exchange membranes (IEM), with focus on the bipolar membrane (BPM).

Three new designs, that assured equally distributed channels for the supply of the solutions, were investigated and compared. Multiple charge and discharge cycles at several current densities were performed. A maximum round-trip efficiency of 51.7 % and an energy density of 1.5 WhL^{-1} were achieved. Furthermore, by improving the cell materials and chemical conditions of work, cycling was proven with a fading of only 1% of the discharge capacity per cycle during 10 charge/discharge cycles.

The data obtained demonstrate that co-ion transportation remains the main challenge to overcome, to increase the battery performance. Therefore, IEM with higher perm-selectivity are needed. Also, a bipolar membrane (BPM) that allows higher discharge current densities must be developed.

Overall, the investigated AB-FB shows promising results that encourage further investigation towards an industrial application. Increasing the round-trip efficiency until at least 70 % will make it competitive with existing technologies.

Keywords: acid base flow battery, bipolar membrane, co-ion transport, round-trip efficiency, coulombic efficiency, cycling, electrical energy storage

Resumo

O rápido crescimento de fontes de energia renováveis cria a necessidade de desenvolver sistemas eficientes de armazenamento de energia elétrica, para assegurar a fiabilidade da rede elétrica. As tecnologias atualmente disponíveis possuem restrições geográficas, questões de segurança ou problemas ambientais. Nesta tese, a bateria de fluxo ácido-base (AB-FB, acid base flow battery) é estudada. A AB-FB consiste numa bateria de fluxo sustentável que utiliza NaCl como solução e membranas de permuta iónica, onde a membrana bipolar é a chave para o funcionamento.

Três novos designs, que asseguram canais de distribuição uniforme para o fornecimento das soluções, são investigados e comparados. Múltiplos ciclos de carga e descarga com diferentes densidades de corrente elétrica são realizados. Uma eficiência energética máxima de 51.7 % e uma densidade energética de 1.5 WhL^{-1} foram alcançadas. Além disso, ao melhorar os materiais da célula e as condições químicas de funcionamento, ciclicidade foi comprovada, com um desvanecimento de apenas 1 % em capacidade de descarga por ciclo durante 10 ciclos de carga/descarga.

Os resultados obtidos demonstram que o transporte de co-iões continua a ser o principal desafio a superar, de modo a aumentar o desempenho da bateria. Assim, membranas com maior seletividade são necessárias. Uma membrana bipolar que permita densidades de corrente elétrica mais elevadas ao descarregar deve ser desenvolvida.

No geral, a AB-FB investigada apresenta resultados promissores que encorajam investigações adicionais para aplicação industrial. Aumentar a eficiência energética até pelo menos 70 % fará com que se torne competitiva com outras tecnologias existentes.

Palavras-chave: bateria de fluxo ácido-base, membrana bipolar, transporte de co-iões, eficiência energética, eficiência de Coulomb, ciclos consecutivos, armazenamento de energia elétrica

The present master thesis was performed in collaboration between the Associated Laboratory for Green Chemistry (LAQV), Faculdade de Ciências e Tecnologia da Universidade Nova de Lisboa (Portugal) and Wetsus, European Centre of Excellence for Sustainable Water Technology (The Netherlands), within the "Blue Energy" theme of Wetsus. The subject studied is part of the BaoBaB project, a European collaborative project.

[http://www.baobabproject.eu/]

Contents

Figures list

Tables list

Abbreviations

AB-FB	Acid Base Flow Battery
AEM	Anion Exchange Membrane
AEL	Anion Exchange Layer
BPM	Bipolar Membrane
CEM	Cation Exchange Membrane
CEL	Cation Exchange Layer
CGFB	Concentration Gradient Flow Battery
ED	Electrodialysis
EES	Electrical Energy Storage
IEM	Ion Exchange Membrane
OCV	Open Circuit Voltage
RED	Reversed Electrodialysis
SOC	State of Charge

Nomenclature

F	Faraday constant [96485 C mol^{-1}]
R	Universal gas constant [8.314 J mol^{-1} K^{-1}]
T	Absolute temperature [K]
z	Ionic charge number
i	Current density [A m^{-2}]
I	Current [A]
E	Voltage [V]
E_m	Membrane Potential [V]
Q	Charge [C]
η_{CE}	Coulombic Efficiency [%]
η_{RTE}	Round-trip Efficiency [%]
R	Resistance [Ω] / Specific Resistance [Ωcm^{-2}]
V	Volume [m^3]
C	Concentration [M]
P_d	Power density [Wm^{-2}]
t	Time [s]
γ_i	Molal activity coeficient
m_i	Molality
ΔG	Gibbs free energy [J]
P	Power [W]
Pd	Power density [W m^{-2}]
N_m	Number of membranes
A	Area [m^2]

1. Framework

Renewable energy sources are growing rapidly to lower the use of fossil fuels that lead to emission of CO_2 [1]. Due to the intermittent nature of wind and solar energy the necessity for the implementation of large scale electrical energy storage (EES) is triggered to ensure the stability and reliability of the electrical power network. The EES will convert the electricity from renewables into a storable form that can be released back to generate electricity when needed [2]. In 2017, still 96% of the global large scale EES systems were comprised of pumped hydropower installations, with a power capacity of 176 GW [3]. Pumped hydropower systems pump water into an elevated reservoir using electrical energy and then recover it by flowing the water down through a turbine. However, this technology has some limitations such as dependence of specific geographic sites, negative environmental impact and low energy densities. The same happens with compressed air energy storage [2]. Another option are batteries, which have higher energy densities and are portable, but until now require scarce and mostly toxic materials that lead to safety concerns and high costs of production [4]. This shows that there is an opportunity for a storage system that can be applied unrestricted of geographical conditions and environmentally safe.

To address this problem pressure retarded osmosis and reversed electrodialysis (RED) for energy storage have been widely studied and gained some attention as a possible solution [5,6]. In the end of the 70's the concept of producing and storing energy from salinity gradients was introduced [7–9]. The concentration gradient flow battery (CGFB) using ion-exchange membranes (IEMs) has been proposed by van Egmond *et al.* [10], which consists of a scalable storage system that performs cycles of charging (electrodialysis, ED) and discharging (RED) creating a battery. The salinity gradient across the diverse compartments, which is created by using two salt solutions with different concentrations, and electro migration promote an ion flux through the IEMs and power is extracted. To note that the CGFB solutions can be made with widely available, therefore cheap, and environmentally friendly materials and it has no location restriction. In addition, it is harmless. The CGFB is not yet feasible economically since the efficiencies reported are still too low [10].

In order to improve power density and energy density and maintaining the same principles the concept of an Acid Base Flow Battery (AB-FB) is introduced also by van Egmond *et al.* [11]. This system, containing bipolar membranes, will be studied in this thesis and the proposition is to expand the potential of the salinity gradient battery by using excess electricity to obtain both a salinity and pH gradient from a salt water body through membrane processes. Some experimental studies have been made until now [11–15]. Thus far, the performance characteristics of the AB-FB need to be improved drastically to obtain an economically feasible EES.

1.1. Research goals

The research goal of this thesis is to improve the round-trip efficiency of the AB-FB by studying new stack designs. The goal is to improve the round-trip efficiency from 13.5% [11] to over 50% to make it acceptable as an EES. Thereby focus is put to the co-ion transport through the membranes, which are not 100% selective. Another focus is the starting point of the system, by comparing starting from 100% State of Charge (SOC) and a complete discharged state (0% SOC). Finally, focus is put towards the concentrations of the acid and base to lower co-ion transport.

2. Introduction

2.1. Electrical Energy Storage System

Nowadays, the reduction of greenhouse gas emissions is one of the main goals towards a more sustainable energy supply. Electricity from renewable energy sources is a solution to this. Between 2000 and 2015 the growth of photovoltaic and wind power went from 1-4 GW to 227 GW and 17 GW to 433 GW [16], respectively. However, such sources, have an intermittent nature. Hence it is necessary to have an EES system that can store the excess energy produced and use it to meet peak demands (peak shaving) and stabilize the variations in the grid which will increase the robustness of low-carbon electricity systems.

Some of the problems with EES have been the high capital cost and low round-trip efficiency. Also, the regulation barrier which does not favour the energy storage, yet, to be able to compete with others in electricity markets [17]. The aim is to achieve competitive conditions with the already known technologies or presenting new ones, that are more efficient and sustainable.

In 2017, 96% of the world capacity of EES was comprised on pumped hydroelectric storage (PHS) with a power capacity of 176 GW, followed by thermal energy storage (2%). Figure 1 shows the installed power capacity world wide of various EES, and Figure 2 shows the power capacity of the electro-chemical storage systems, in which AB-FB is a part.

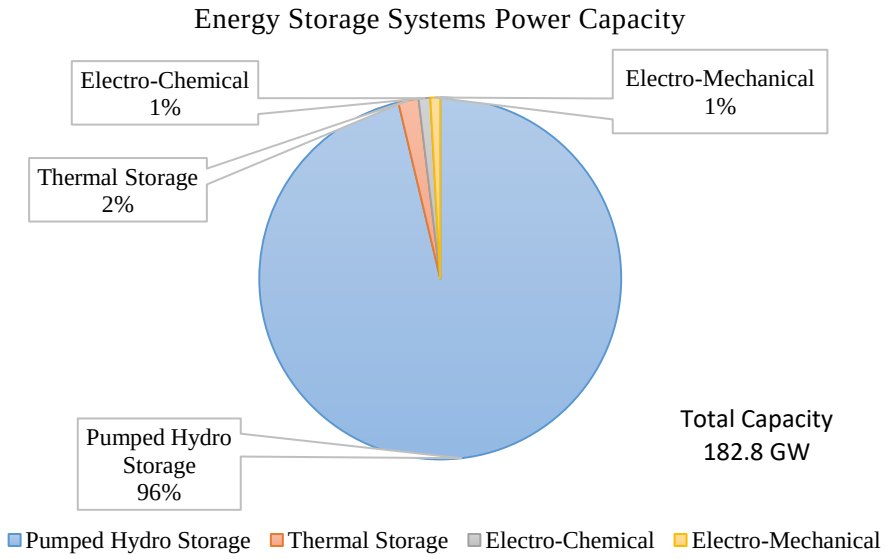

Figure 1 - Installed power capacity of various EES globally in mid-2017. The electrochemical storage power is equal to 1 % of the total (1.82 GW) [3].

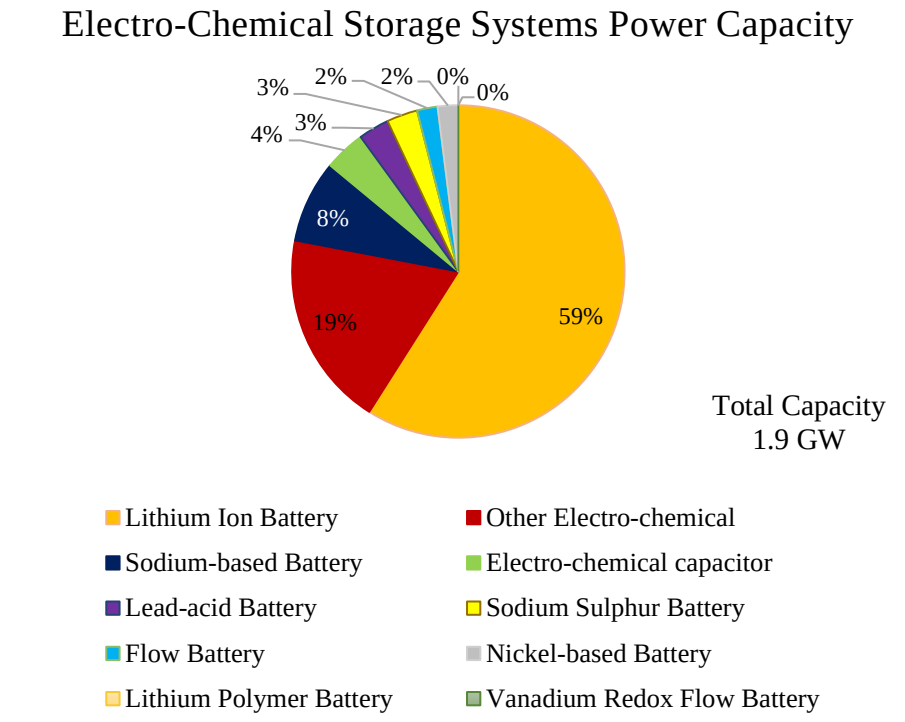

Figure 2 - Installed power capacity of various electro-chemical storage systems globally in mid-2017 [3] *with Li-ion covering 59%.*

It is possible to classify the EES technologies by power rating and discharge duration, as shown in Figure 3. Technologies with long discharge duration and high-power rating, such as PHS, can provide services like balancing to the transmission system operator and energy management. Others with shorter discharge duration and lower power rating, for example flywheels, supercapacitors or batteries, are more suitable for the provision of services to distribution network operators and residential users. Although all of these technologies are EES, they can have different employments to do so [17].

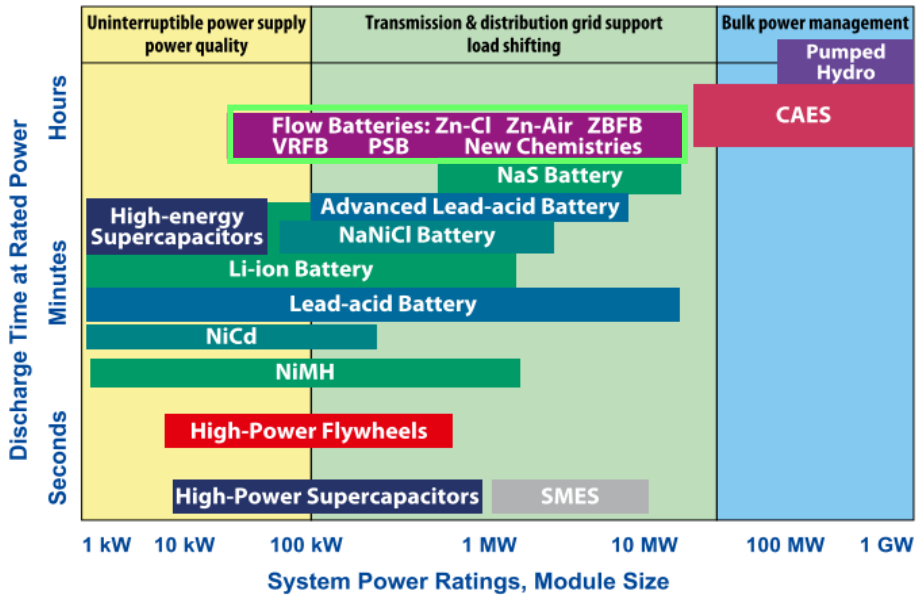

Figure 3 - Electricity storage technology options to support the systems by discharge time (seconds to hours) and system power rating (kW to GW) [3].

To better understand the differences between these technologies, some relevant EES were selected and will be described briefly.

Pumped Hydroelectric Storage [18]

PHS is the most important EES technology in the world with 96% of all the electrical storage capacity installed. A typical PHS plant is constituted by two water reservoirs at different elevations. During off-peak electricity demand hours, the energy is used to pump water into the higher reservoir and later during peak hours, the water can be released to the lower reservoir generating electricity. The electricity is generated when the water passes through a turbine. The amount of energy stored is dependent of the height difference between reservoirs.

The life time of this technology is around 40 years and presents low self-discharge. The main disadvantages are the geographical restriction, the time of construction, a high capital investment and environmental impact. The round-trip efficiency is between 70 % and 87 %.

Compressed Air Energy Storage [18]

The energy is stored in the form of pressurized air (until 200 bar). During low power demand periods, the excessive electricity is driven through a motor unit that runs a chain of compressors for injecting air into a storage vessel. To release the electricity the air is released, heated and passed through turbines. The Compressed Air Energy Storage (CAES) can be built to have a small or a large scale capacity.

Similar to PHS it has some geographical restrictions that will influence the main investment. The self-discharge rate is negligible. The energy efficiency in this technology needs improvement since it is situated around 40 – 70 %.

Lithium-ion Battery [18,19]

In a Li-ion battery, the cathode is made of a lithium metal oxide and the anode is made of graphitic carbon. The electrolyte is usually a non-aqueous organic liquid containing dissolved lithium salts. The battery operates through the shuttle of lithium ions between electrodes.

The battery life time is estimated of 15 years, similar to other batteries described further. The self-discharge rate is around 1 % daily and, the energy efficiency is one of the highest of over 85 %. It has a high initial capital cost limiting extensive application. Situations of charging and discharging randomly and frequent charging can restrict the life time of the battery. Some safety risks are associated to lithium ion because of increasing temperature during functioning which can be responsible for internal short circuits.

Lead-acid Battery [18,19]

The lead-acid battery components are a cathode made of PbO_2, an anode made of Pb, and the electrolyte is sulfuric acid. It is the most mature battery technology and has low cost.

The disadvantages are that it does not work properly in cases of deep charging and discharging, losing capacity. The round-trip efficiency can be lower than for the lithium ion battery with a range of 63 % to 90 %.

Sodium-sulphur Battery [18,19]

Sodium-sulphur batteries use molten sodium and molten sulphur as the positive and negative electrodes, respectively. Beta alumina is used as solid electrolyte and separator between electrodes. The working temperature is 300 – 350 ºC.

By working at high temperatures, an extra vacuum system is required. Safety issues can be found in here, for example if the ceramic tubing ruptures it causes short circuits that can lead to fires. An advantage is the high recyclability of the battery since it uses inexpensive and non-toxic materials. The self-discharge is negligible, and it has a round-trip efficiency between 75 % and 85 %.

Nickel-cadmium battery [18]

Nickel-cadmium batteries use nickel hydroxide and metallic cadmium as the two electrodes and as electrolyte an aqueous alkali solution.

Cadmium and nickel are both heavy metals, making the battery non-environmentally friendly. The battery suffers from memory effect, the capacity is affected if the battery is repeatedly charged after being partially discharged. The daily self-discharge is less than 1%, and the round-trip efficiency is reasonable (60 % - 83 %).

Zinc Bromine Flow Battery [18]

This hybrid flow battery consists of two aqueous electrolyte solutions of zinc and bromine stored in external tanks. The solutions flow through the stack, which contains ions exchange membranes and electrodes, while charging/discharging. Zinc ions are converted to metallic zinc and bromine is converted to bromide, and the other way around.

Bromine is toxic so there are some safety issues regarding this flow battery. The main drawbacks are material corrosion and high energetic costs of production. As vanadium redox flow battery, having the electrolytes stored in different tanks assures small self-discharge rate. The round-trip efficiency is comprised between 65 % and 85 %.

Vanadium Redox Flow Battery [18–20]

The vanadium redox flow battery uses vanadium redox couples (V^{2+}/V^{3+} and V^{4+}/V^{5+}) in sulphuric acid solution to storage energy in two electrolyte tanks. The electrolytes are separated by an ion exchange membrane. The electron exchange takes place at the graphite felt electrodes in the aqueous phase.

One advantage of this redox flow battery is that cross contamination of the electrolytes does not damage the system since the metal ions are of the same element. The high costs of the electrolyte are a limiting factor for industrialization, related to lack of vanadium availability. Since the electrolytes are stored in different tanks the self-discharge rate is small, and the reported round-trip efficiency is from 71 % to 85 %.

All Iron Flow Battery [21–23]

The iron flow battery uses iron redox couples (Fe/Fe^{2+} and Fe^{2+}/Fe^{3+}). The iron electrode utilizes plating and dissolution of iron and the positive electrode uses a carbon structure to oxidize and reduce iron cations which are in solution. A plastic separator is used to separate both electrolytes.

All iron flow battery presents inexpensive reactants and materials, and it is environmentally friendly. The round-trip efficiency reported is over 77 %.

Hydrogen storage and fuel cell [18]

Hydrogen energy storage systems use two separate processes for storing energy and producing electricity. A water electrolysis unit is commonly used to produce hydrogen which can be stored in high pressure reservoirs and/or transmitted by pipelines. When using stored hydrogen for electricity generation, a fuel cell is used. Fuels cells can convert chemical energy of hydrogen and oxygen to electricity. It is released in electrical energy and heat during the discharge process.

Fuel cells are easy scalable and compact. Reported round-trip efficiencies are situated between 20 % and 66 % which means some improvement is still needed. These cells use precious materials such as palladium and platinum. And the storage of large amounts of hydrogen brings the risk of fire or explosion. Regarding daily self-discharge it is considered almost zero.

Concentration Gradient Flow Battery [4,10]

The CGFB consists of two tanks with sodium chloride solutions, pumps, electrodes and ion exchange membranes. By using the process of electrodialysis a chemical potential difference is first achieved and using reverse electrodialysis electrical energy can be retrieved.

CGFB round-trip efficiencies are very low compared with the other systems (15 % - 40 %). It is a sustainable battery by using abundant earth compounds and is easily scalable.

Acid Base Flow Battery [11]

The AB-FB consists of four solution tanks, where acid, base, salt and redox solutions are stored. Alike the CGFB it comprises ion exchange membranes, including a bipolar membrane, pumps and electrodes. The principle is to take advantage of the pH gradient that is achieved between the acid and base compartment.

Until now round-trip efficiency is very low (13.5 %) but this technology is very recent and there is opportunity to improve. The flow battery does not represent any safety risk or environmental danger, and it is scalable.

Important parameters of the EES systems are power rating, response time, energy density, power density, operating temperature, self-discharge, round-trip efficiency, lifetime, cycles, power cost, and energy cost. The most important parameters out of these listed are energy density, power density and round-trip efficiency as these parameters give the primary information about energy storage technologies, as presented in Table 1 [24]. In addition, a sustainability parameter is inserted. Nevertheless, it is important to study the period of construction, capital cost, flexibility of the installation and environmental issues related to the technology.

To summarise and compare all the EES systems described above, Table 1 is presented. In Table 1, each line represents one type of EES. These technologies were chosen to compare for being already mature/commercialized or for showing promising performance.

Table 1 - Comparison of the different electrical energy storage systems (*) estimated, ( ) the technology respects, ( ) the technology near-respects

	Energy density	**Power Density**	**Round-trip efficiency**	**Sustainability**
	(W h/L)	(W/L)	(%)	References
Pumped Hydro (PHS)	0.2 – 2	0.1 – 1.5	70 – 87	[18,25–27]
Compressed Air (CAES)	2 – 6	0.2 – 2	40 - 70	[18,25–27]
Li-ion	200 – 400	1300 – 10000	85 – 98	[18,19,25–27]
Lead-acid	50 – 80	10 – 700	63 – 90	[18,19,25–27]
Sodium-Sulfur	150 – 300	120 – 180	75 – 85	[18,19,25–27]
Nickel-Cadmium	15 – 150	80 – 600	60 – 83	[18,26,27]
Zinc-Bromine	30 – 60	< 25	65 – 85	[18,26,27]
Vanadium Redox Flow	16 - 35	< 2	71 – 85	[18,19,25–27]
All iron flow battery	-	5 (W/m^2)	> 77	[23]
Hydrogen Fuel Cell	500 – 3000	> 500	20 – 66	[18,25,26]
Concentration Gradient Flow Battery (CGFB)	0.1 – 1.3	0.01 – 0.2*	15 – 40*	[10,28]
Acid Base Flow Battery (AB-FB)	2.9	2.1[1]	< 13.5	[11]

[1] Calculated from 3.7 Wm^{-2}. Membrane and compartment thickness: 0.18 cm. $P_d = \frac{3.7}{100 \times 0.018} = 2.05\ WL^{-1}$

Compared to other batteries, the AB-FB has a lower energy density, although the value of 2.9 W h/L has prospect to improve. Whilst comparing the energy density with PHS or CAES, both mature technologies, the AB-FB achieves the same or higher energy density.

In terms of round-trip efficiency, the AB-FB exhibits the lowest value of all the technologies, which can be explained by the fact that the technology is still under development and there is prospect for enhancement.

Sustainability refers to the development that meets the needs of the present without compromising the ability of future generations to meet their own needs [29]. In this parameter, there are five technologies that abide with it. Sodium-sulphur battery is considered sustainable due to the abundancy of the components to make it, but regarding safety, it can be very dangerous since pure sodium can spontaneously burn. Pumped hydro systems, can be considered sustainable since the energy is generated by the water movement, but the construction of this system can have environmental impacts and presents some danger for the workers building it. The geographic restriction remains a drawback for this technology. Concerning AB-FB, there are no safety or sustainability risks. The fact of using acid and base, in case of leakage of one the other can be released to neutralise and all the materials to make it are abundant [11]. Therefore, only three technologies really cover the ideal conditions to reach a completely sustainable, environmentally friendly and safe energy storage system. These technologies are the all iron flow battery, the CGFB and the AB-FB.

One more advantage presented by the AB-FB is the easy addition of more cells between the two electrodes. The AB-FB is made of compartments in the middle of the electrodes and to achieve higher voltages the addition of more membranes and creation of more compartments is easily achievable. This is not possible for other systems, due to their construction type (PHS and CAES, for example) or constitution (Lithium-ion is mostly not bipolar).

2.2. System components

2.2.1. Monopolar Membranes

Monopolar membranes take part in the AB-FB process and can be classified as cation- or anion- exchange membranes, referred as CEM and AEM, respectively (both represented in Figure 4). A CEM is a monopolar membrane with a negatively charged groups fixed to a polymer matrix, which allow cations to pass through it as counter-ions, excluding anions as co-ions. This exclusion occurs since the co-ions have the same electrical charge as the fixed group. This is called the Donnan exclusion. The cation exchange fixed groups are sulfonic acid, carboxylic acid, phosphonic acid, monosulfate ester groups, and others [30].

Meanwhile, an AEM has the opposite functionality, with a positively charged groups fixed to a polymer matrix which allow anions to pass through and exclude cations. Some anion exchange fixed groups are primary, secondary, and tertiary amino groups, quarternary ammonium groups, quarternary phosphonium, and other groups that provide positively fixed charge [30].

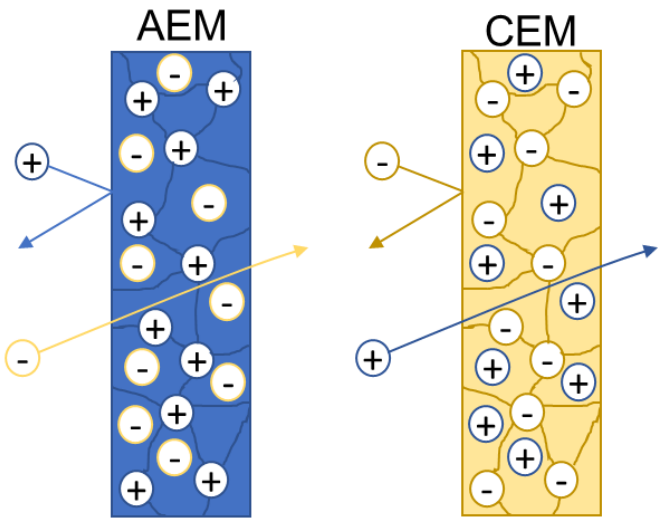

Figure 4 - Two types of monopolar membranes. On the left: anion-exchange membrane, on the right cation-exchange membrane. Fixed charges are the same colour as the background of the membrane.

2.2.2. Bipolar Membrane

The key component of acid base flow battery is the bipolar membrane (BPM). It is in the BPM that the water splitting occurs originating acid and base. In the next paragraphs, components, techniques of preparation and characteristics of bipolar membranes will be discussed.

Bipolar Membrane Components

The main characteristics for a BPM are: high water dissociation efficiency, low electrical resistance,

low co-ion transport rates, high ion-selectivity, long life time, and good chemical, thermal and mechanical stability [31,32].

The BPM is composed by three parts, the anion exchange layer, the cation exchange layer and the contact region between them, known as bipolar junction. Its typical function is to dissociate solvents, when under reversed bias. Until now only two solvents are reported to dissociate in BPM: water (H_2O) and methanol (CH_3OH) [33,34]. Water dissociation in the BPM has been widely studied and it is the phenomenon occurring in the AB-FB.

Regarding the anion and cation layers, they should allow sufficient water flux from the compartments into the junction to replenish the water consumed by the water dissociation reaction. These layers should transport the water splitting products (protons and hydroxyls) and being selective, avoiding co-ion transportation. The fluxes of co-ions are responsible for salt contamination of the products, and, when in an AB-FB system, lowering the round-trip efficiency [35]. Co-ion transport however becomes very limited if the BPM is used at the water dissociation conditions i.e. at least a voltage of 0.8 V is applied across the BPM. The anion and cation layers contact with the base and acid compartment, respectively; thus, they must be stable in strong base or acid solutions. The charged groups mostly used in membranes are sulfonate groups which provides the fixed negative charge of the cation layer and quaternary amine groups that carry the positive fixed charge in the anion permeable layers. These groups are permanently dissociated covering almost all the pH range and achieve a high conductivity of the ion selective layers [32].

Bipolar Junction

As referred before, in the middle of the BPM is the essential part of its functioning, the so called bipolar junction (also called transition region or contact region). The bipolar junction normally is an additional layer between the anion and cation layers and, in some cases, can be a part of either the anion or the cation layer at the contact interface of the two layers. To enhance the desired water dissociation reaction, catalysts are added to the bipolar junction. The reaction of the water dissociation is accelerated about 50 million times [36]. An example of a catalytic reaction that occurs can be seen in equation 1.

$$\begin{array}{l} Fe^{3+}+H_2O \rightarrow FeOH^{2+}+H^+ \\ \underline{FeOH^{2+} \rightarrow Fe^{3+}+OH^-} \\ H_2O \rightarrow H^+ + OH^- \end{array}$$

Equation 1

It has been reported that weak ion exchange groups have catalytic activity as well [32]. Some examples of weak cation exchange groups are carboxylate or phosphate; and some examples of weak anion exchange groups are tertiary and secondary amines.

If an electric potential is applied an electric field is imposed across the bipolar membrane. Charged species will move from the transition region out of the BPM, as shown in Figure 5. The protons and

hydroxyl ions removed from the transition region are substituted by the water dissociation equilibrium [36]. In reversed conditions during discharge, protons and hydroxyl ions go towards the bipolar junction for water formation. In this situation the reversed current applied is limited due to the "ballooning" effect. When the formation of water inside the BPM has a higher rate than the release rate to the outside of the BPM, it can delaminate or balloon [37].

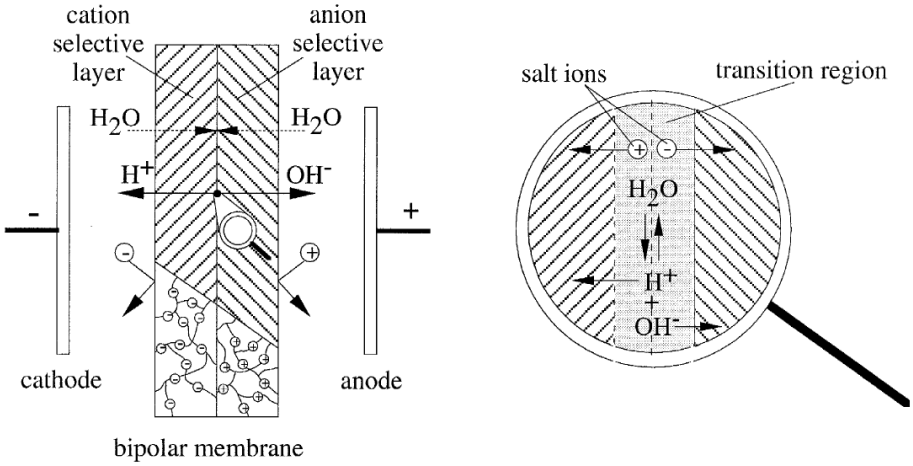

Figure 5 - Schematic drawing illustrating the function and structure of a BPM [36].

Bipolar membrane preparation

For the BPM preparation the commonly reported steps are shaping the interface structure (the initial ion exchange layer is roughened), introducing the catalyst, and establishing the contact (the ion exchange layer with opposite charge is applied) [32].

In 1993, H. Strathmann *et al.*, showed three types of preparation: laminating the anion and cation exchange layer back to back, casting the cation exchange layer on top of a previously prepared anion exchange membrane and bipolar multilayer membranes prepared from identical monopolar films. The results were better for the last case, in which the potential drop was at least twice less than in the other two cases (of 1.5 V). [31]

Also, in the same year, Simons [38] reported a new method of preparing. Where separate anion and cation exchange membranes are joined together using an alkaline solution of a metal salt as a binder. This binder lowers the resistance of the interface.

In 2016, Pan *et al.* [39] published a new method of preparation based on electrospinning followed by hot-pressing. This production method has the advantage of controlling the thickness of each layer by adjusting the electrospinning time. The results compared with a BPM produced by casting were good. The new method presented the same yield regarding the production of acid and base, but the potential drop associated was much lower.

Finally, the latest BPM procedure was introduced by Shen *et al.* [37], where the membrane is made by electrospinning of single and dual fibre, followed by dimethylformamide vapor exposure and hot-pressing. A high interfacial 3D region for water splitting junction is created. With this characteristic it is possible to achieve a reversed current density (water formation) of 1100 Am^{-2} without membrane damage, while current commercial membranes only have a stable performance until 200 Am^{-2}.

2.3. Electrodialysis and Reverse Electrodialysis

ED is a membrane-based process, in which ions are transported due to a voltage applied between the electrodes. Figure 6, shows the principle of conventional ED. The membranes between the electrodes are AEMs and CEMs, that are arranged in an alternating pattern. When the voltage is applied, anions (-) start to move in the direction of the anode, while cations (+) move to the opposite direction towards the cathode. Anions will cross the AEMs and will be retained by the CEMs. Likewise, cations will cross the CEMs and will be retained by the AEMs. The result will be one stream rich in ions, the concentrate, and another depleted of ions, the diluate. The repeating unit (one AEM, one CEM and two compartments) is referred to as a cell pair inside the ED stack [30,40,41].

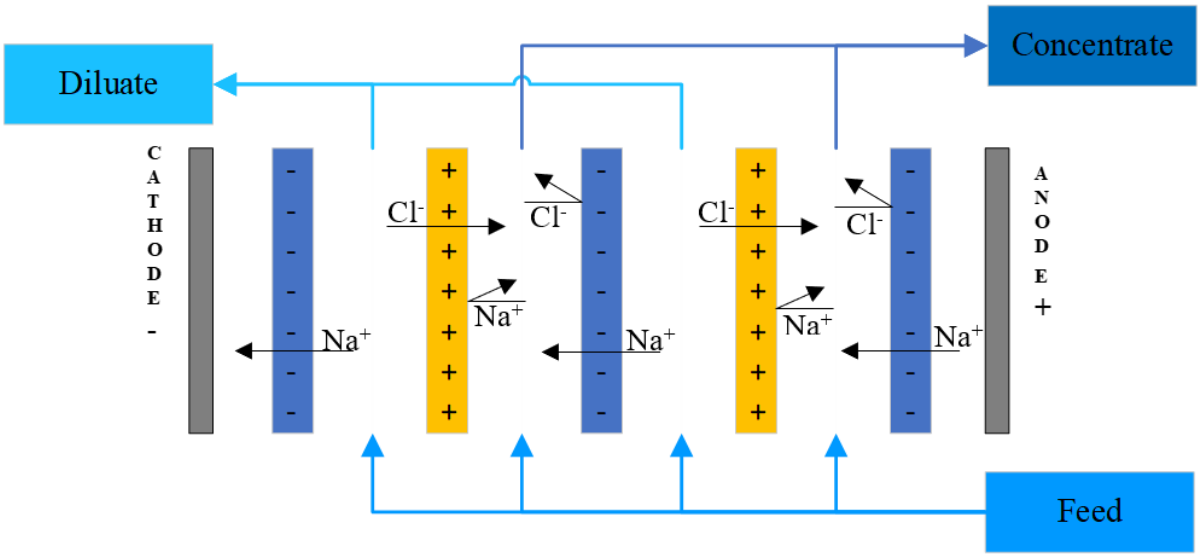

Figure 6 - Schematic diagram of the principle of electrodialysis.

The main application for electrodialysis is water desalination. It is also used in salt production, water reuse and food processing.

While ED uses energy to produce a diluate and a concentrated salt stream, RED generates electrical energy by mixing fresh water and seawater in a similar setup to ED. By mixing these two streams the chemical potential difference can be harvested. The chemical potential causes the ion transportation through the membranes from the concentrated solution to the diluted solution. Cations will permeate through the CEMs and anions through the AEMs. The electro-neutrality throughout the system is

obeyed, using appropriate redox pairs, via oxidation at the anode and via reduction at the cathode. Electrons are transferred from the anode to the cathode via an external electrical circuit. The electrical current and the potential difference over the electrodes can be used to generate electrical power [42].

Besides the conventional ED/RED processes with monopolar membranes, a BPM and a compartment can be added to the cell pair. One standard application is to produce acids and bases by ED. By combining both techniques, the AB-FB is created. ED is used to charge and create the pH gradient, and RED is used to discharge using the pH gradient. The working principle is explained in chapter 2.5.

2.4. Background of Acid Base Flow Battery (AB-FB)

The first proposal of an energy storage system through salinity was published by Weinstein and Leitz [7], in 1976. Three years later, Ramp [43], introduced the AB-FB concept as secondary battery powered by forced ionization, however the article focuses on depolarising bipolar electrodes with a palladium foil instead of the BPM. In the 80's, Emrén and Holmström [12], published a study using the scheme of AEM – BPM – CEM with an energy efficiency reported less than 0.1 %. Zholkovskij et al. [13], modelled a AB-FB based on ideal bipolar membranes under different regimes (charge, discharge and self-discharge) and experimented in a three-compartment electrodialysis cell with a BPM. They charged only up to 0.03 M acid/base and the specific energy reported was up to 0.1 Wh kg^{-1}. They concluded that membranes with better permselectivity were needed. In the same year, Pretz and Staunde [14], published an experimental study focusing on RED (discharging) assuming non-ideal permselectivity and showed that permselectivity of the membranes decreased with the increase of the concentration. Maximum discharge efficiencies of less than 1%, with 1 M of acid and base, were reached. In 2016, a study by Kim *et al.* [15] showed a cell design following a patent [44] using two electrodes of porous carbon felt with platinum-coated titanium. Finally, the last study on this subject was published by van Egmond *et al.* in 2017 [11]. They report an energy density of 2.9 W h L^{-1} and round-trip efficiencies up to 13.5%, concluding that the AB-FB requires improvements.

2.5. AB-FB Working Principle

The AB-FB is based on a reversible acid-base reaction. Opposing to typical or other redox flow batteries, the AB-FB has some advantages, such as, not requiring precious, toxic or scarce materials. Furthermore, for the AB-FB the solution used is NaCl solution meaning it can be seawater, which is abundant and cheap. The number of electrodes is reduced to two and up to hundreds of membrane cell pairs in series can be put between them. Besides, the electrodes do not need to be (noble) metals. They can be made of carbon or graphite which is environmentally friendly [45]. It is also important that the energy spent to produce the battery is small. The AB-FB has the potential to reach high energy storage on invested values, since it uses natural and cheap materials. In addition to these advantages, one important characteristic of this battery is safety. Fire or explosion hazard is negligible. Contamination of soil, water or

air is very unlikely, even if the acid (base) tank leaks or ruptures, it could be rapidly neutralized by unloading the corresponding base (acid) tank [12].

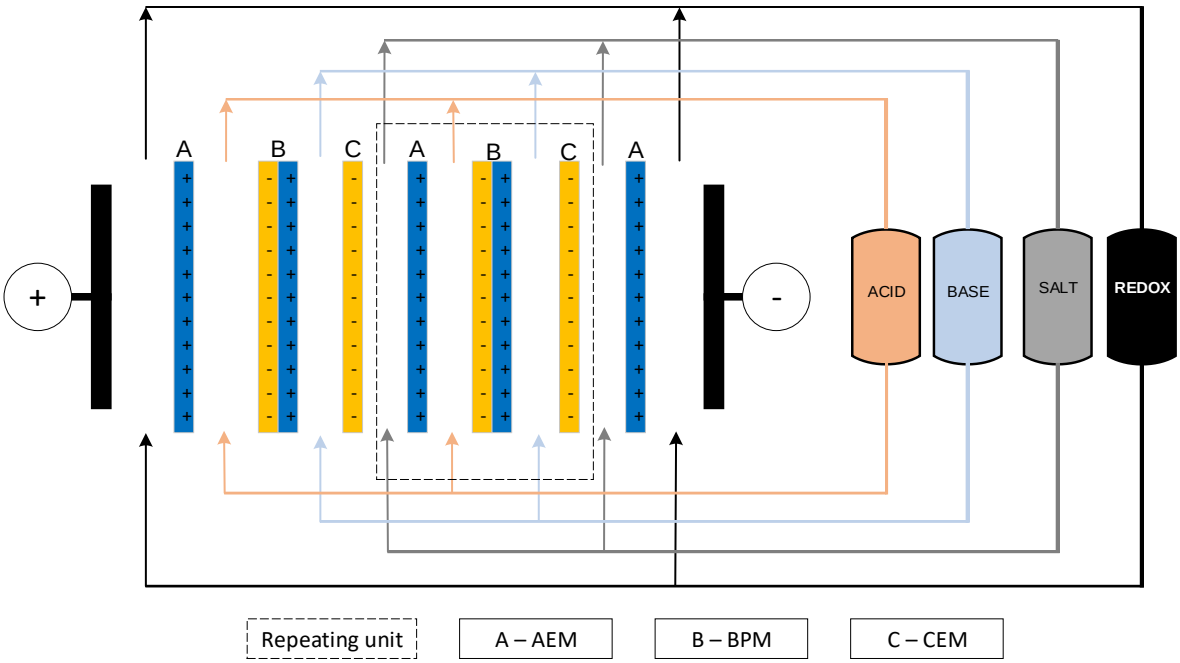

Figure 7 - Schematic of an acid base flow battery. On the left side, the membrane assembly. On the right side, the reservoirs with solutions. The membranes between the two electrodes are stacked in a repetitive manner, ending with one extra anion membrane as shielding membrane to separate the redox solution.

In Figure 7, it is possible to observe the schematic structure of an AB-FB. On the left side the stack assembly is given and on the right side are shown the reservoirs with the four solutions. The stack is composed by bipolar, cation and anion ion exchange membranes. These are sequentially placed (AEM, BPM, CEM …). A spacer is placed between membranes which is permeable to the electrolyte solutions, the space created is called a compartment. Between the two electrodes many cells pairs are present (represented as repeating unit in Figure 7). One cell pair is composed of three membranes (AEM, BPM, CEM) and three compartments (one for each solution, acid, base and salt). An extra AEM is added as shielding membrane for the redox solution. The solutions are pumped through the compartments and go back to the reservoirs. The fourth reservoir called redox contains the solution that assists the redox reaction at the electrodes. It is only pumped through the two electrode compartments and converts the ionic current through the membranes into an electrical current at the electrodes.

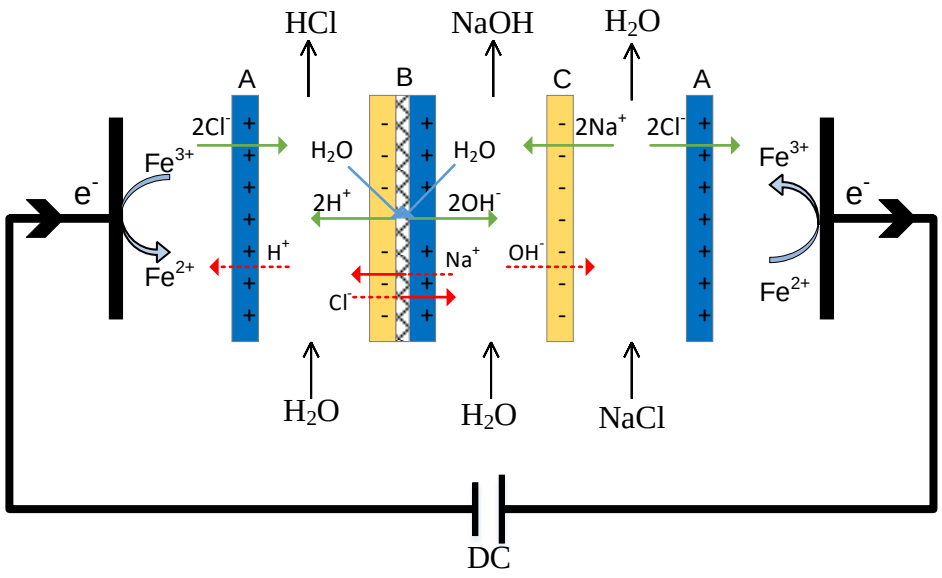

Figure 8 - Electrodialysis, charging the AB-FB system using a DC power supply.

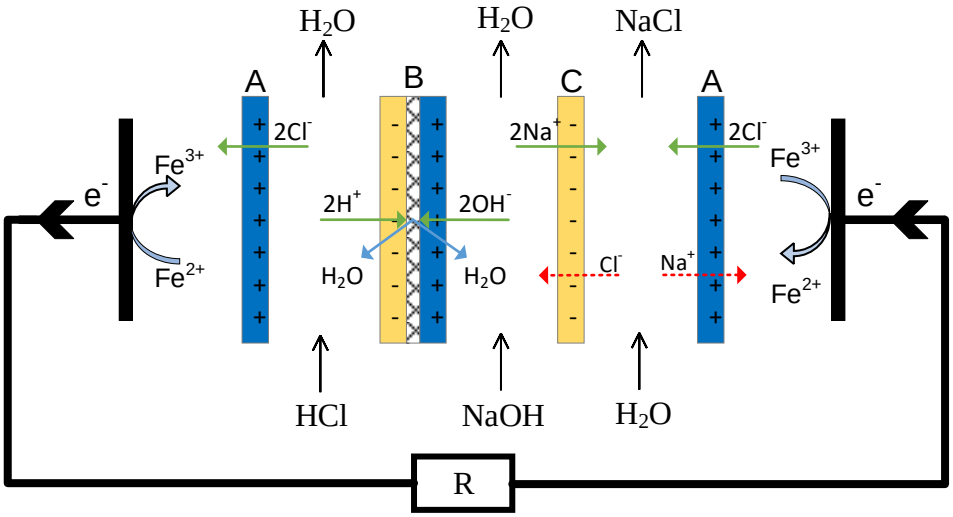

Figure 9 - Reverse Electrodialysis, discharging the AB-FB system across a load R.

To understand the functioning of the AB-FB, Figure 8 represents the charging step and Figure 9 the discharging step. From left to right the compartments are denoted as: redox, acid, base, salt and redox. The BPM is delimited by the acid and base solutions. The green arrows represent counter-ion transportation, the red arrows represent co-ion transportation, note that other forbidden paths can occur. And the blue arrows represent the formation and dissociation of water.

For the charging phase the electrodialysis process is carried. The compartments compositions are a concentrated salt compartment and in extreme conditions pure water in the acid and base compartments. This extreme state (0% SOC) is unwanted because pure water is a poor current conductor. A constant current is applied to the electrodes and ions in solution and ions inside the membranes will start to move according to the electrical field. Here, the left electrode works as cathode and the right as anode. The

anions will move towards the anode, through AEMs. And oppositely the cations will move in the cathode direction. With this, the acid compartment gains chloride ions and protons generated from the water dissociation in the bipolar membrane, which results in hydrochloric acid. The base compartment enriches in sodium ions and hydroxyls (also generated in the BPM) and sodium hydroxide is formed. The salt compartment is the Cl^- anion and Na^+ cation donor and becomes diluted. To note that none of the compartments should get depleted of ions. It is important to define the SOC interval of functioning, since 0% and 100% SOC are considered as extreme conditions.

At the end of the charging phase, the base reservoir is alkaline, the acid reservoir is acidic and the salt concentration in the salt reservoir decreases. The energy is stored by the pH gradient that is created between the acid and base solutions. The difference in water activity between the acid and base solution should be kept at the minimum because it improves the efficiency of the process, prevents ballooning of the BPM and balances the transportation of water generated to both solutions in contact with the BPM [46].

For discharging the conditions are reversed and the reverse electrodialysis process is carried. By applying the reverse current, the electrical energy can be retrieved. Now the electrode processes are reversed, at left the anode and at the right the cathode. Here, the water dissociation effect is null, so the current is primarily carried by the present ions. The protons and hydroxyls diffuse into the BPM to convert into water. The accumulation of ions in the BPM makes the Donnan exclusion less effective, and some of the accumulated ions cross freely into other compartments as co-ions. This phenomenon prejudices the AB-FB functioning. The concentrated acid and base solutions become diluted and the salt solution recovers the sodium and chloride ions.

The desired starting point is to start from salt water in all compartments, but from a point of view of better performance, having acid and base in the respective compartments and start with discharge will avoid unwanted ions like Na^+ in the acid compartment and Cl^- in the base compartment. For example, sodium ions in the acid compartment will compete with protons to go inside the bipolar membrane while discharging.

The results of the study made by van Egmond *et al.*, 2017, by deep charge and discharge the AB-FB, with up to 1 M of acid and base, were: power densities up to 3.7 W m^{-2} per membrane, energy densities up to 2.9 W h L^{-1}, and round-trip efficiency up to 13.5%.

2.6. AB-FB Properties

2.6.1. Open circuit voltage

The open circuit voltage (OCV) is the voltage present in a battery when it is not connected to any load. The OCV is an important parameter for batteries since it represents the maximum voltage difference

when there is no current and the circuit is not closed. The voltage of the cell, that corresponds to the OCV, can be calculated from the Nernst equation (equation 2).

$$E_m = \alpha_m \frac{RT}{zF} \ln\left(\frac{\gamma_{i,1} m_{i,1}}{\gamma_{i,2} m_{i,2}}\right) \quad \text{Equation 2}$$

Where E_m is the membrane potential, α_m is the membrane selectivity, R is the gas constant, T is the absolute temperature, z is the ionic charge number, F is the Faraday constant, $\gamma_{i,1}$ and $\gamma_{i,2}$ are the molal activity coefficient at each side of the membrane, $m_{i,1}$ and $m_{i,2}$ are the molality at each side of the membrane. For monopolar membranes the concentration is between compartments and for bipolar membranes the concentration is between the compartment and the anion and cation exchange layers (AEL and CEL, respectively).

For the theoretical potential, the concentration of the solutions can be considered equal to their activity, by assuming ideal solutions, which can be a coarse approach since the activity value normally is different of 1.

For the calculation of the cell potential the following constraints were used $R = 8.314\, JK^{-1}mol^{-1}$, $T = 298.15\, K$ and $F = 96485.33\, C\, mol^{-1}$. It is known that when the water dissociation occurs the concentration in the junction is 10^{-7} M because it only contains pure water [36]. The potentials were calculated for each membrane using 0.5 M HCl and 0.5 M NaOH.

Bipolar membrane:

$$E_{AEL} = \frac{RT}{zF} \ln\left(\frac{[OH^-]_{bp}}{[OH^-]_{base}}\right) \approx \frac{RT}{-F} \ln\left(\frac{10^{-7}}{0.5}\right) = 0.3963V \quad \text{Equation 3}$$

$$E_{CEL} = \frac{RT}{zF} \ln\left(\frac{[H^+]_{acid}}{[H^+]_{bp}}\right) \approx \frac{RT}{F} \ln\left(\frac{0.5}{10^{-7}}\right) = 0.3963V \quad \text{Equation 4}$$

Anion exchange membrane:

$$E_{AEM} = \alpha_m \frac{RT}{zF} \ln\left(\frac{[Cl^-]_{salt}}{[Cl^-]_{acid}}\right) \approx \frac{RT}{-F} \ln\left(\frac{0.25}{0.5}\right) = 0.0178\, V \quad \text{Equation 5}$$

Cation exchange membrane:

$$E_{CEM} = \alpha_m \frac{RT}{zF} \ln\left(\frac{[Na^+]_{base}}{[Na^+]_{salt}}\right) \approx \frac{RT}{F} \ln\left(\frac{0.5}{0.25}\right) = 0.0178V \quad \text{Equation 6}$$

$$OCV = E_{AEL} + E_{CEL} + E_{AEM} + E_{CEM} \quad \text{Equation 7}$$

Gathering equation 3 to 6, equation 7 is presented. The theoretical voltage of the cell is then calculated using equation 7. If the same concentration is used in the three compartments, the potential is only

created in the BPM ($E_{AEM} = E_{CEM} = 0$). And the OCV is equal to 0.7926 V. If there is a difference of concentration in the salt compartment, of 0.25 M, for example, the cell potential can reach 0.8282 V.

2.6.2. Charging time

Given the solution concentration (C) and volume (V) the theoretical charge can be calculated as shown in equation 8.

$$Q_{CH} = C_{solution} \times V_{solution} \times F \quad \text{Equation 8}$$

Where, F is the Faraday constant (96485.3 C mol^{-1}). By setting a constant current and dividing the charge for it, the theoretical time of charging is obtained (equation 9).

$$t_{CH} = \frac{Q_{CH}}{I} \quad \text{Equation 9}$$

In the experimental work the charging time used was the theoretical value as calculated. In case of 0.5 L of 0.5 M HCl, the capacity is equal to 6.7 Ah.

2.6.3. Coulombic efficiency

Coulombic efficiency (η_{CE}) is the ratio of the total charge extracted from the battery over the total charge put into the battery over a charge/discharge cycle. It describes the charge efficiency by which electrons are transferred in a system facilitating an electrochemical reaction. It can be calculated through equation 10.

$$\eta_{CE} = \frac{Q_{DCH}}{Q_{CH}}.100\% \quad \text{Equation 10}$$

Until now the maximum coulombic efficiency achieved for this system was 27% [11].

2.6.4. Round-trip efficiency

The round-trip efficiency is the ratio of the energy recovered from the battery over the energy put in. It is the most important parameter in energy storage systems. With high round-trip efficiency, low losses occur during charge and discharge. The value of the round-trip efficiency for each cycle (charge and discharge) can be found through equation 11.

$$\eta_{RTE} = \frac{\int_{t_1}^{t_2} I_{DCH}(t)E_{DCH}(t)dt}{\int_{t_3}^{t_4} I_{CH}(t)E_{CH}(t)dt}.100\% \quad \text{Equation 11}$$

The voltage is changing over time; therefore, it is necessary to integrate. On the other side the applied current for charge and discharge is kept constant, I_{CH} and I_{DCH} can be put in front of the integral. This way equation 11 can be simplified.

For an economically feasible energy storage system, 50 % of round-trip efficiency should be the minimum value acceptable. The average of the EES round-trip efficiency of commercial systems is over 70 % as shown before.

2.6.5. Energy Density

To show the amount of energy a given system can store, energy density can be used. It can be used per mass (specific energy) or volume (volumetric energy density). To compare with other energy storage systems, the AB-FC is calculated in terms of volumetric energy density.

The maximum energy content, also known as Gibbs Free Energy (ΔG) is given by equation 12.

$$\Delta G = -n \times F \times \Delta E \qquad \text{Equation 12}$$

Where n is the number of moles of electrons transferred in the reaction, F is the Faraday constant and ΔE is the total cell voltage.

Using 0.5 M of HCl, n equals to 0.5 mol and ΔE equals to 0.7926 V (chapter 2.6.1.), the ΔG is 38213 J. The theoretical energy density (Wh L^{-1}) of the acid base flow battery, is the ΔG value divided by the 3 solutions used (acid, base and salt). The energy density of the AB-FB in these conditions will be 3.5 Wh L^{-1}.

To reach higher energy densities, the solutions concentrations can be increased. For 1 M of HCl the energy density reaches 7.4 Wh L^{-1}. To note that higher concentrations may have a negative effect on the battery performance and real energy density, due to higher chance of co-ion transport.

2.6.6. Internal Resistance

Resistance is the opposition that a material offers to the flow of direct current.

The stack resistance, in Ohms, can be calculated from the IV curve, Figure 10, using the difference of potential over the difference of current. Or by using the difference between the OCV and the initial discharge voltage divided by the correspondent currents. The second approach was used in the results section. Equation 13 represents the formulation above.

$$R = \frac{\Delta E}{\Delta I} \qquad \text{Equation 13}$$

To give a comparable value to other systems the resistance is multiplied by the electrode area.

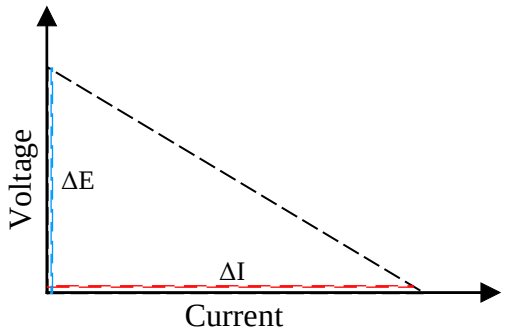

Figure 10 - Typical IV curve without electrode limitation.

2.6.7. Power Density

Power relates to the amount of energy transferred per unit of time. The power output of the AB-FB can be found from the Kirchhoff's law [47]:

$$P = I^2 R_{ext} = \frac{OCV^2 R_{ext}}{(R_{int}+R_{ext})^2}$$ Equation 14

To achieve maximum power output the external resistance (R_{ext}) must be equal to the internal resistance (R_{int}), resulting in equation 15. It is assumed no limitation of electrode reactions.

$$P_{max} = \frac{OCV^2}{4R_{int}}$$ Equation 15

The power density, P_{dmax}, is obtained with equation 16.

$$P_{dmax} = \frac{P_{max}}{N_m A}$$ Equation 16

Where N_m is the number of membranes and A is the effective membrane area.

3. Materials and Methods

This chapter will describe the materials used in the experiments and the methods implemented to achieve the results.

3.1. Materials

The AB-FB stack used in this work uses the same membranes as van Egmond *et al.* [11] but is not similar in terms of construction of the cell.

The flow battery is assembled as represented in Figure 11. It comprises 2 AEM – fumasep FAB® reinforced 75 µm (Fumatech, Germany) membranes; 1 CEM – fumasep FKB® reinforced 130 µm membrane (Fumatech, Germany) and 1 BPM – fumasep FBM reinforced 130 µm (Fumatech, Germany) membrane. The FAB is chosen for being a good proton blocking membrane. The properties of the ion exchange membranes can be found in Table 2.

Table 2 - Properties of the ion exchange membranes as used [48–50]

Membrane	**Fumasep FAB-PK-75**	**Fumasep FKB-PK-130**	**Fumasep FBM**
Type	AEM	CEM	BPM
Thickness (µm)	75	130	130 – 160
Permselectiviy (%)	93 – 98	96 – 99	-
Conductivity ($mS.cm^{-1}$)	0.7 – 1	2 – 8	-
pH stability (at T=25ºC)	0 – 14	1 – 14	0 – 14
Resistance ($\Omega.cm^2$)	2.9 – 5.2	2.5 – 5	< 3

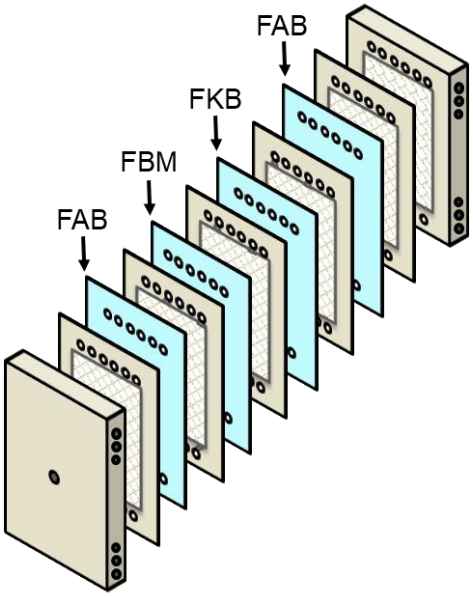

Figure 11 - Overall configuration of the stack (membranes configuration). End plates and electrodes in the extremities, and a sequential distribution of spacers/gaskets and membranes in between.

The unit cell is made up from one membrane of each type and the extra AEM is used as shielding membrane to separate the redox compartment. In all experiments only one single cell is used. For pumping peristaltic pumps were used (MasterFlex ® L/S ®, Cole Palmer, The Netherlands). The flowrates are described in each design.

Figure 12 shows schematically the experimental set-up for the AB-FB. Pictures can be found in appendix A.

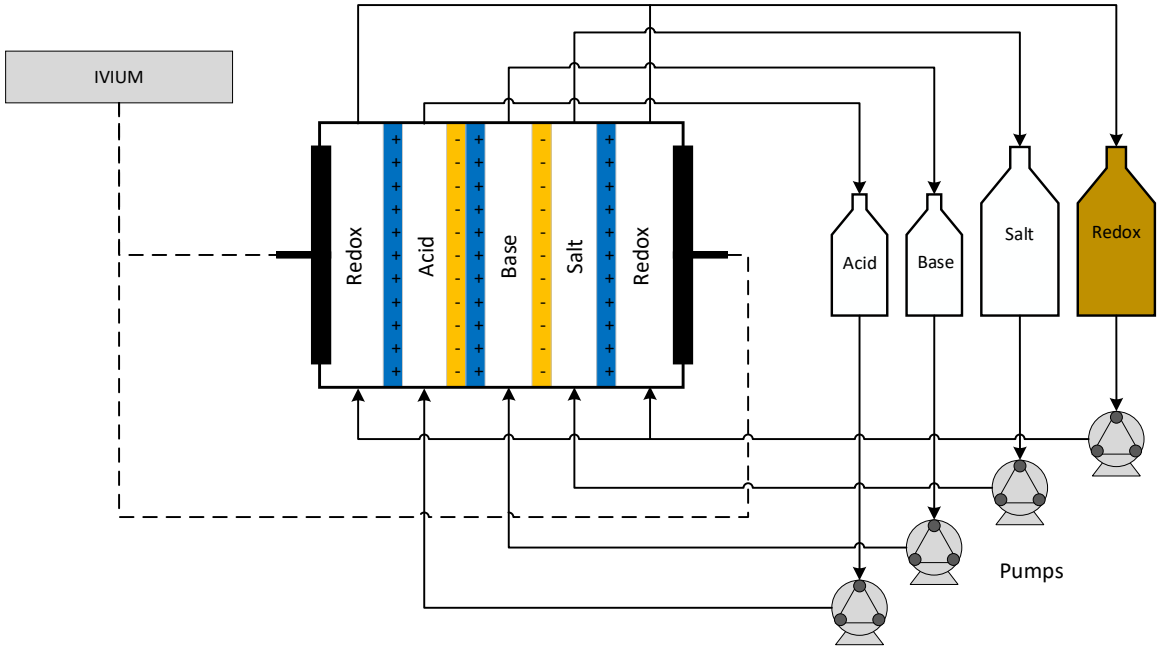

Figure 12 - Scheme of the set-up of the acid base flow battery. The IVIUM potentiostat is connected to the electrodes (anode and cathode), pumps are used to pass the solutions through the stack, each for the respective compartment. The bottles are connected to the stack with PP tubes. Pump tubing was Neoprene.

The chemicals used to prepare the solutions can be found in Table 3.

Table 3 - Chemicals used to prepare the solutions

Name	Molar Mass (g/mol)	Manufacturer
Sodium Chloride	58.44	VWR Chemicals
Sodium Hydroxide	40.00	VWR Chemicals
Hydrochloric Acid	36.46	VWR Chemicals
Iron (II) Chloride tetrahydrate	191.81	VWR Chemicals
Iron (III) Chloride	162.20	Boom BV

3.2. Stack design

To achieve proper sealing, better performance, homogeneous flow distribution and a stable system, three different designs were used in this work, each one described below.

Design 1: Spacers with 450 µm thickness and 51% of open area (SEFAR PETEX®, Switzerland) are used to create the compartments between membranes. Silicone gaskets (500 µm, Eriks BV, The Netherlands) are used to seal the spacer channel. The silicone material however varied in thickness as much as 50 microns for a single gasket. Also, the silicone material contained parts of a filler material similar to calcium hydroxide or calcium carbonate. The electrodes (20*20 cm^2) are Titanium mesh coated with 2.5 µm Pt (Magneto Special Anodes B.V., The Netherlands). The electrodes are connected to a potentiostat (IviumStat.XR, Ivium Technologies, The Netherlands). First 1 mm silicon gaskets and 1 mm spacers were used at the end plates, but since the fitting for the electrodes at the end plates was more pronounced than it should (electrodes were positioned below the end plate plateau where the end gasket was placed), graphite felt (with 95 % volume porosity) was later added as a spacer to fill-up the electrode volume, replacing the previous spacer. The membranes and gaskets were held together with two acrylic plates (end plates) and pressed with bolts, using an average 8 Nm torque. The major improvement of this design compared to the previous in literature [11] is the improved distribution of the flow path.

Design 2: Integrated spacer/gaskets (AquaBattery, The Netherlands) with higher quality silicone rubber are used to seal and create the compartments between membranes and end plates, with a thickness of 450 µm. Graphite felt is used at the end plates with an integrated spacer/gasket. This design is an improvement of design 1 that showed internal leakage.

Design 3: Electro MP Cell (ElectroCell, Denmark) was used as stack. Fluoro-elastomeric rubber (FPM, Viton) with 1 mm thickness is used as gaskets for sealing, guaranteeing a uniform thickness and chemical stability against strong acid and strong base. A 7 mm PP spacer with defined flow distribution that assures a homogenous flow is used. The electrodes (10*10 cm^2) are Titanium (grade 1) with 2.5 µm Pt coating and stainless steel end plates to close and pressurize the stack. Two layers of graphite felt at each electrode are added to lower the redox over potential at the electrodes. The electrodes are connected to a potentiostat (Vertex.S, Ivium Technologies, The Netherlands).

3.3. Experimental procedure

3.3.1. Underwater assembly

For the design 1 and 2, the ion exchange membranes used have an effective area of 0.04 m^2. Having this in consideration, the shrinking and swelling effects by exposing them to the solutions are notorious. Further, the BPM requires to be wetted at any time. The BPM is made of three different layers with different shrinking rates, upon drying its properties are lost and there is no recovery, since micro-cracks occur [50]. To make sure the membranes are completely conditioned, a pre-treatment in 0.5 M NaCl for at least 24 hours is performed. After this treatment, the membranes do not swell anymore and can be cut. For these reasons, it is necessary to assemble the stack underwater, meaning in a tank filled with 0.5 M NaCl solution covering the surface of the stack (Figure 13). Underwater assembly went smoothly without further problems.

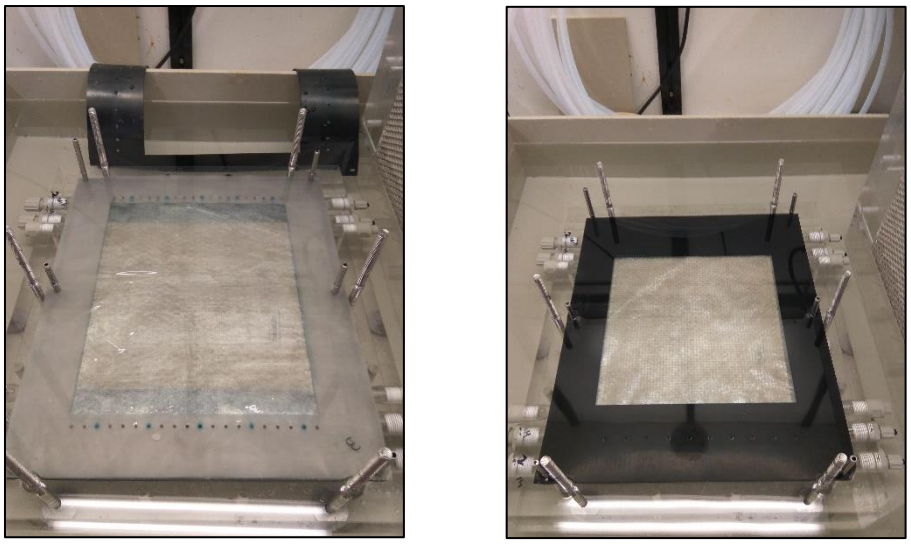

Figure 13 - Underwater assembly of design 1.

3.3.2. Leakage test

After assembly of the cell, a leakage test is made using 0.5 M NaCl. By providing the same solution in all compartments, water transportation by osmosis does not occur and the solution bottles should maintain the liquid volume. In this way it is possible to check internal leakages. In case of external leakage, which can be seen by eye, it is safer to use NaCl solution rather than acid or base.

3.3.3. Design 1 settings

This design was used to test the resistance of the electrodes. No other tests were possible with design 1 as result of internal leakage caused by poorly defined thickness of the silicone rubber material available (500 µm silicone rubber, ERIKS BV., The Netherlands). The silicone rubber appeared to have thickness variation of at least 50 microns for the size of the gasket used. Also, unexpectedly, $CaCO_3$ was added by the manufacturer to prevent sticking during the production process. As known $CaCO_3$ reacts with strong acid and a consequence the structure of the silicone rubber becomes fragile and distorted.

The flow rate used was 70mL/min (or 1.87 cm/s). The solutions were 0.5 L 0.5 M HCl, 0.5 L 0.5 M NaOH, 0.5 L 0.25 M NaCl and 0.8 L 0.25 M $FeCl_2$ with 0.25 M $FeCl_3$ and 0.1 M HCl, for acid, base, salt and redox compartment, respectively. The redox solution was based on the article by Veerman *et al.* [51] which proposes the system (electrolyte and electrode) and classifies it is the most promising one. The battery started in the charged state and a constant current density of 25 $A.m^{-2}$ without graphite felt and 25 or 50 $A.m^{-2}$ with graphite felt was applied to discharge.

3.3.4. Design 2 settings

The design 2 was used to show improvement of the round-trip efficiency of the AB-FB and the possibility of scale-up from previous work [11]. Multiple experiments were conducted using constant currents that are described in Table 4. The flow rate was 70 mL/min (or 1.87 cm/s). After the cell voltage reached

zero volt during discharge, the experiment was stopped. The discharge current was limited to a maximum value of 2 A (50 $A.m^{-2}$), as the bipolar membrane might suffer delamination at higher current densities. The charge current was limited by the potentiostat maximum current of 2 A. For each experiment the acid, base and salt solution were renewed (apart from experiment 5 which was conducted right after experiment 4).

Table 4 - Current applied at charge and discharge in design 2

Discharge/Charge	1 A	1.5 A	2 A
1 A	1		
1.5 A		2	3
2 A		4	5

3.3.5. Design 3 settings

To demonstrate cycling with the AB-FB, cell design 3 was used. Also, for comparison with design 2 and literature. The solutions used were 0.5 L 0.5 M HCl, 0.5 L 0.5 M NaOH, 1 L 0.5 M NaCl and 0.6 L 0.5 M $FeCl_2$ with 0.5 M $FeCl_3$ and 0.1 M HCl, for acid, base, salt and redox compartment, respectively.

For proof of cycling, two experiments were conducted, first with a flowrate of 220 mL/min (or 0.53 cm/s) and second with 500 mL/min (or 1.2 cm/s). Each experiment lasted for 10 charge/discharge cycles by first charging with 1 A and then discharging with 0.5 A (both constant currents). The solutions at start corresponded to a charged state (100% SOC), so a discharge with 0.5 A was made before starting cycling.

To retrieve data to compare with previous designs, 5 experiments were conducted using the constant currents in Table 5. The flow rate used was 500 mL/min (or 1.2 cm/s).

Table 5 - Current applied at charge and discharge in design 3

Discharge/Charge	0.375 A	0.5 A	1A
0.375 A	2	4	
0.5 A	5	3	1

3.3.6. IC / ICP test

At the end of each cycling experiment, samples were taken from each bottle to check the composition of the solutions and to see the amount of co-ion transportation, following Wetsus protocol for IC for Na^+ and Cl^- and ICP for Fe.

4. Results and Discussion

4.1. Resistance of the electrodes

While working with only one cell pair, the electrodes resistance affects the performance of the AB-FB. By adding a graphite felt material at the electrodes, while trying to improve design 1, it was discovered that the resistance of the electrodes decreased by 60 %. It is possible to see this effect in Figure 14, where the resistance is compared between the average of three experiments without graphite felt with the average of four experiments with graphite felt. Data for Figure 14 can be found in appendix B. The resistance was calculated according to equation 13 (chapter 2.6.6.).

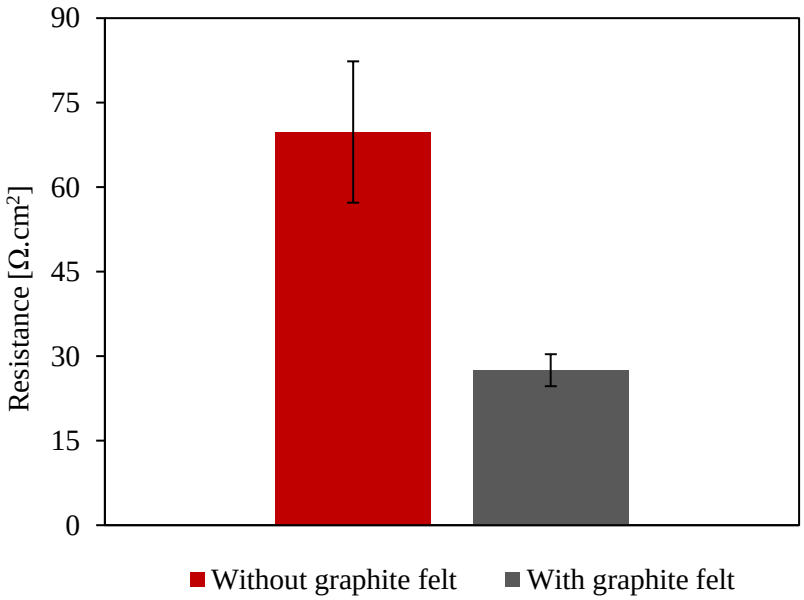

Figure 14 - Stack resistance difference by applying one layer of graphite felt at each electrode.

The addition of graphite felt resulted in a larger contact area with the redox solution due to the increased electrode surface.

Another way to lower the resistance effect of the electrodes is adding more unit cells between the electrodes. The electrode resistance is the same, but the impact of it on the stack performance will be divided by all the cells and becoming negligible. The resistance of the membranes and compartments will have a bigger impact.

The graphite felt was applied to the following experiments.

4.2. Round-trip efficiency at different current densities

With design 2, independent cycles were run at different current densities. Figure 15 shows the cell voltage of the stack versus time, and Table 6 shows the range of current densities applied.

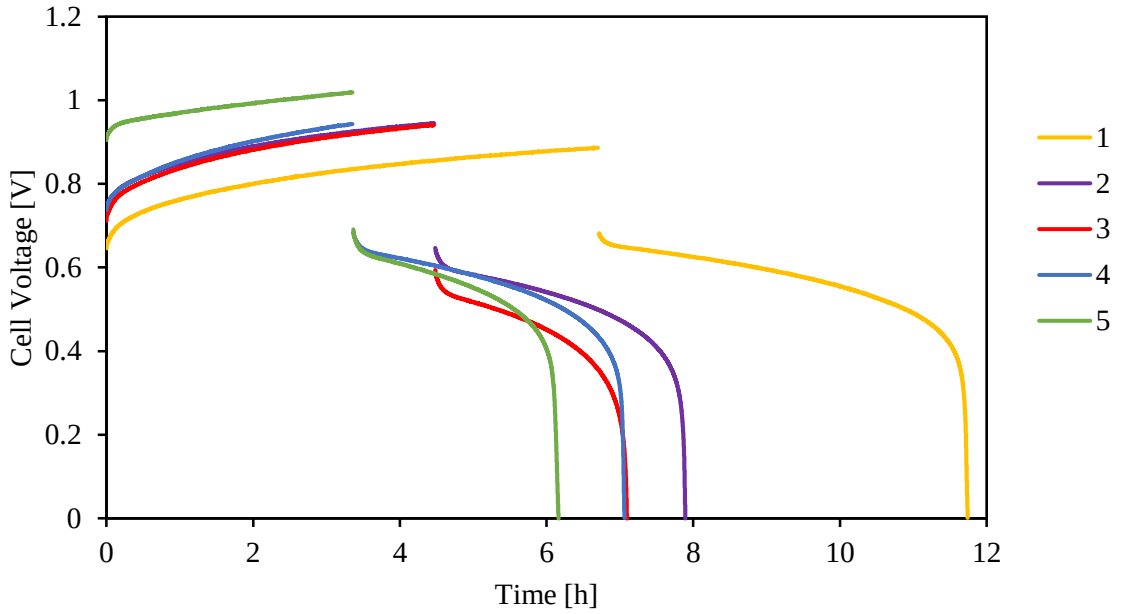

Figure 15 - Cell voltage during charge and discharge over time, for five different current densities combinations.

Table 6 - Current density applied in charge and discharge in each experiment

Experiment Nr.	**1**	**2**	**3**	**4**	**5**
i_{Charge} **[A m^{-2}]**	25	37.5	37.5	50	50
$i_{Discharge}$ **[A m^{-2}]**	25	37.5	50	37.5	50

At higher current density the time of charge and discharge is reduced. From experiment 1 with 25 Am^{-2} to experiment 5 with 50 Am^{-2}, the time to complete a cycle is almost reduced to half. Experiment 5 has a higher cell voltage during the charging step due to the usage of the same solution as experiment 4. Consequently, the initial concentration of the solutions for experiment 5 can differ slightly from the others, creating higher resistance. The accentuated potential drop at the end of each discharge is because most of protons and hydroxyls already became water at the bipolar membrane.

To compare the performance of the different experiments, the coulombic efficiency (η_{CE}) and round-trip efficiency (η_{RTE}) were calculated, according to equation 10 and 11, respectively. In Figure 16 it can be seen the high coulombic efficiency (75 % – 83 %) and moderate round-trip efficiency (39 % – 52 %).

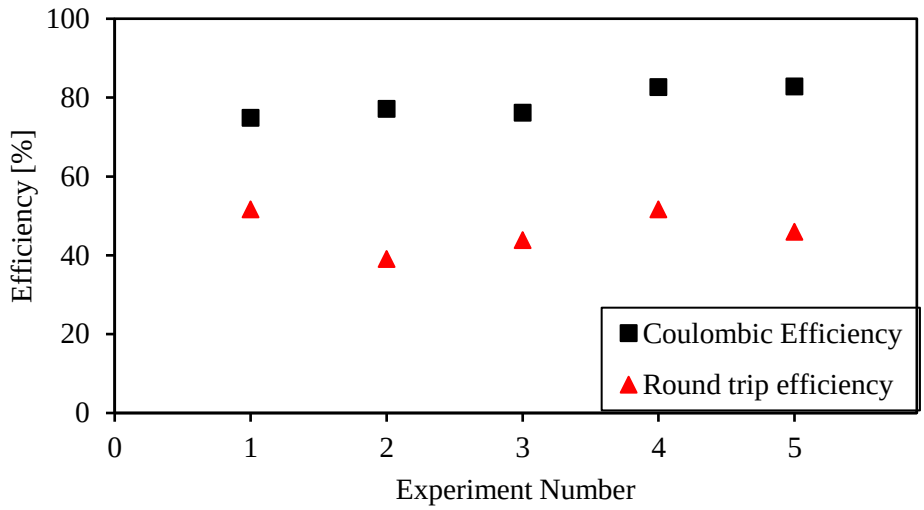

Figure 16 - Coulombic efficiency (η_{CE}) and round-trip efficiency (η_{RTE}) of 5 experiments with design 2.

Regarding coulombic efficiency, the experiments at higher charging current density (4 and 5) show the best results (82.8 %), which can indicate a faster charge will contribute to a good performance. The reason is that the charge current density needs to be such that water dissociation occurs inside the bipolar membrane. In general, the coulombic efficiency increases with increased current densities, mainly in charging.

The stack resistance for experiment 4 and 5 is lower (Table 11, appendix C).

The round-trip efficiency (51.7 % for experiment 1 and 4) surpassed the 50 % mark. At lower charge current density co-ion transport of Na^+ and Cl^- will occur through the bipolar membrane since the voltage for water splitting has not been reached. During discharge less voltage loss will occur if discharged at a lower current density and this explains the higher round-trip efficiency for experiment 1. It is noted that experiment 5 may not have reached the 50 % mark due to the fact of using the same solutions as experiment 4.

It is interesting to see between experiment 3 and 4, which have opposite charge/discharge current density, end up discharging around the same time, as seen in Figure 15. Figure 16 shows that experiment 4 has around 6 % higher coulombic efficiency and 8 % higher round-trip efficiency compared to experiment 3.

As a result, it was shown that higher current densities provide better coulombic efficiency combined with good round-trip efficiency.

4.3. Cycling of Acid Base Flow Battery

One important feature of batteries is to maintain the same performance over consecutive cycles. A cycle is considered as a charge and a discharge of the battery.

The stack used corresponds to design 3 (chapter 3.2.).

To prove the cycling concept of the acid base flow battery, an experiment with 10 cycles was performed, lasting around 7.5 days. The time of charge was defined through equations 7 and 8 in 2.6.2. Figure 17 shows the cell voltage during 10 consecutive cycles. To charge a current density of 100 Am^{-2} was applied and to discharge a current density of 50 Am^{-2} was applied.

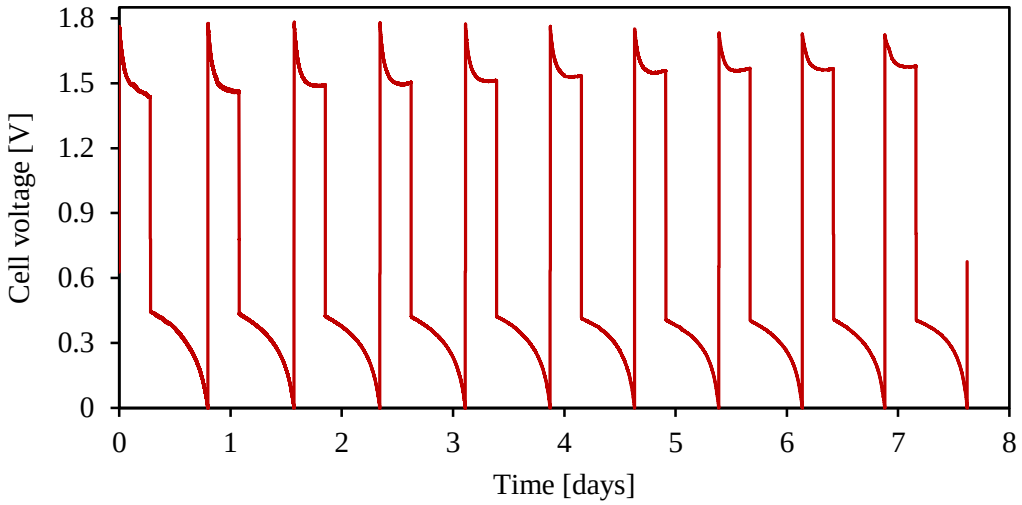

Figure 17 – Cell voltage during cycling for 10 cycles.

There is no significant difference between the cycles, which suggests after 10 cycles the AB-FB could continue operating for more cycles. After discharge until the cell voltage reached zero, the system re-stored until almost the original OCV value. The reason for this is because when the cell reached zero volts, this value included an ohmic voltage drop. Also, the depletion of the boundary layers will diminish after discharge. When current is being applied the concentration near the membrane will become much lower than the bulk concentration.

Figure 18 shows the cycles overlap, where the cell voltage (V) is plotted versus time (h).

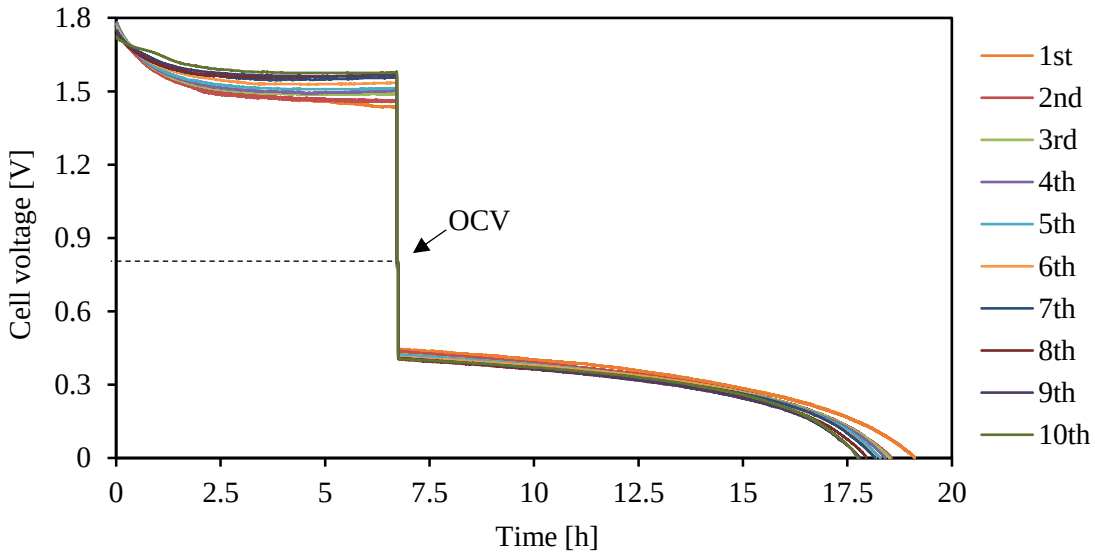

Figure 18 - Cycles overlap. First, charging with 100 A m^{-2} for 6.7 hours, followed by 1-minute OCV and discharging with 50 A m^{-2} until the cell voltage reaches zero. The experiment was performed continuous (no interruptions between cycles).

The average OCV was 0.790 V which agrees with the theoretical OCV of 0.7926 (chapter 2.6.1). The voltage in the beginning of the charging process was higher due to the low concentration of ions present in the acid and base compartment resulting in a higher resistance. Comparing between cycles, the cell voltage while charging increased each cycle most likely because of co-ion transportation of Na^+ and Cl^- and, for the same reason, while discharging it decreased. The first cycle has a slightly longer discharge time because of fresh solutions of pure 0.5 M HCl and 0.5 M NaOH. The co-ion transportation of Na^+ and Cl^- occurs due to the low current density used to charge. Using a low current density to charge, the water splitting voltage across the BPM junction is not reached. Figure 19 shows schematically what occurs during charging at the BPM.

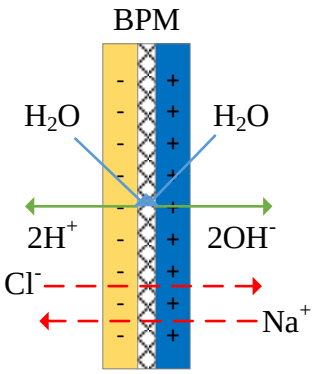

Figure 19 - Schematic of co-ion transportation of Na^+ and Cl^- through the BPM.

It was observed that some iron species from the redox solution were passing through the AEM to the acid compartment. To check the diffusion of iron ions from the redox compartment to the adjacent compartments (acid and salt), an ICP test was made and the results are presented in Table 7.

Table 7 - ICP results for total iron concentration after cycling

	Iron concentration [mg L^{-1}]
Acid	13500
Base	0
Salt	18.7
Redox	79900

Initially iron ions were only present in the redox solution (0.5 M $FeCl_2$ and 0.5 M $FeCl_3$). After 3 cycles the acid solution started to become yellowish and the iron concentration measured in the end of the experiment (Table 7) confirmed the presence of iron. The high concentration of iron in the redox compartment might facilitate the introduction of iron to the acid compartment. For the salt compartment the behaviour was different since the higher pH did not allow the presence at a high concentration of free iron ions in it. The final iron concentration in the salt solution is negligible compared with the concentrations in the acid and redox compartment.

A possible explanation for this transport of iron species through the AEM is that $FeCl_4^-$ is formed in the redox compartment and diffuses through the AEM while charging. When discharging the iron can go to the BPM creating some irreversible loss due to the binding of Fe^{3+} in the cation membrane part of the BPM. To prevent this from happening, there is have two options: i) to add NaCl to the redox solution and ii) to increase the salt solution volume.

Furthermore, the transportation of Cl^- ions and Na^+ ions was analysed. Table 8, shows the initial (calculated) and final (through IC measurement) concentrations of the ions in each compartment.

Table 8 - Chloride and sodium concentration before and after cycling in each compartment

Compartment	Ion	Initial concentration [M]	Final concentration [M]
Acid	Cl^-	0.5	0.28
	Na^+	0.0	**0.16**
Base	Cl^-	0.0	**0.14**
	Na^+	0.5	0.38
Salt	Cl^-	0.5	0.55
	Na^+	0.5	0.58
Redox	Cl^-	0.1	0.50
	Na^+	0.0	0.03

At the end of cycling, the AB-FB was discharged. This corresponds with diluted acid and base solutions and a concentrated salt solution. As Table 8 shows, the concentration of Cl^- and Na^+, in the acid and base solutions respectively, decreased as expected. The presence of Na^+ and Cl^- (values in **bold**), in the acid and base solutions respectively, indicates co-ion transport. This will influence the battery performance. Sodium ions will compete with protons at the CEM part of the BPM during discharge and the hydroxyls ions compete with chloride ions at the AEM part of the BPM during discharge. The redox

compartment acquires five times more the initial chloride concentration, possibly due to decomplexation of iron species.

The values of pH and conductivity of each compartment after 10 cycles were measured and are presented in Table 9.

Table 9 - pH and conductivity after 10 cycles for each compartment

Compartment	pH	Conductivity [mS/cm]
Acid	1.113	46.4
Base	13.062	60.9
Salt	2.437	54.0
Redox	0.856	68.4

The drastic drop of pH in the salt compartment (from 7 to ~ 2.4) indicates that leakage of protons occurs through the AEM. The acid and base compartment after discharge are slightly diluted (pH difference is less than 1 in both cases). The reason to not reach a pH value closer to neutral is because most of the energy of the AB-FB is stored in the higher pH difference between compartments. At pH 2, of the acid compartment, the energy left to recover is negligible, because most protons and hydroxyls are used from the acid and base compartment [11].

Figure 20 represents the resistance of the stack over the cycles. It is calculated from the cell voltage drop at the start of discharge after one minute OCV, using equation 13 (chapter 2.6.6.).

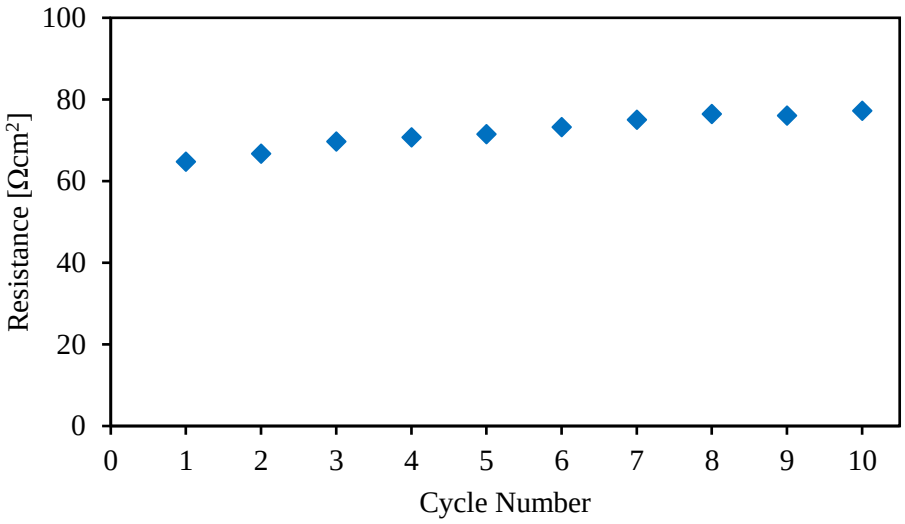

Figure 20 - Stack resistance at the start of discharging in each cycle.

After the evidence presented above, Figure 20 shows that the stack resistance is increasing over the cycles possibly due to the binding of Fe^{3+} inside the CEM part of the BPM or due to the presence of Na^{+} in the acid and Cl^{-} in the base solution. Only degradation of the membranes or the change of composition

of the solutions could be the cause for this ohmic resistance increase, no other characteristics change during cycling.

Degradation of the membranes is discarded because more experiments were conducted posteriorly with the same membranes but with new solutions and the resistance value was similar to cycle 1.

The coulombic efficiency (η_{CE}) and round-trip efficiency (η_{RTE}) are plotted in Figure 21. These parameters were calculated for each cycle, using equations 9 and 10, respectively.

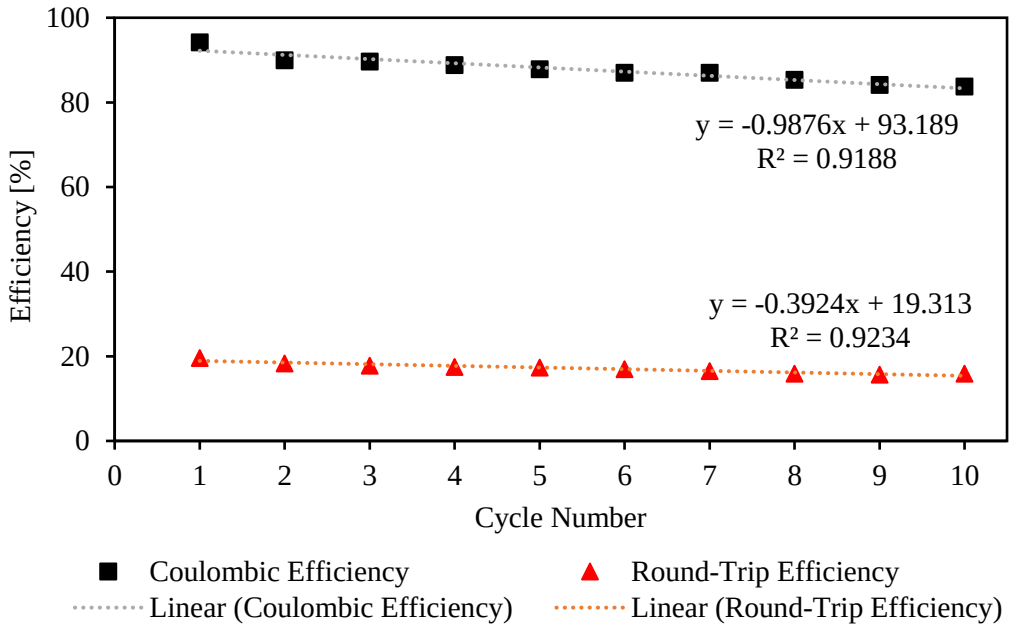

Figure 21 - Coulombic efficiency (η_{CE}) and round-trip efficiency (η_{RTE}) over 10 cycles. Charging with 100 Am^{-2} and discharging with 50 Am^{-2}. ElectroCell with FAB, FKB and FBM fumatech membranes.

High coulombic efficiencies were reached (94 % - 84 %) but low values of round-trip efficiency were achieved (20 % - 16 %) due to the large thickness of each compartment. The spacer thickness was 7 mm, which creates a high resistance in the compartments. The slight decrease in both parameters through each cycle can be explained by co-ion transportation of Na^+ and Cl^-, as described above. The concept of cycling is proven to be feasible with design 3, the stack design, including materials, and membrane selectivity are the foundation for a stable AB-FB.

By adding a trend line to each parameter in Figure 21, it is possible to see the fading rate. The coulombic efficiency has a fading rate of **1 %** over each cycle and the round-trip efficiency a **0.4 %** fading rate over each cycle.

In appendix D, results from a second experiment are shown where the depletion of ions in the salt compartment resulted in the malfunction of the AB-FB. It is important to have a larger volume of salt (in this study it was used 2 times more, but it can be used a higher ratio) to guarantee that no depletion occurs and conductivity in the salt compartment is maintained.

To note that after the last discharge the measurement was finished but pumping was not stopped right away. This led to water transportation through the membranes to balance concentration differences between compartments, and consequently the volumes in the bottles changed.

4.4. Comparison between designs

In this section a comparison between three different designs is discussed. Two from the experimental work (design 2 and 3) and one from literature [11].

It is important to show here how each design works and how a homogeneous flow distribution was achieved. Design 2 has a distributor for each solution with 5 entry points. In this way, the solutions divide equally over the entire membrane area. This can be seen in Figure 22 and Figure 23. In design 3, the spacers assure the distribution by having 2 mixing zones for the solutions to go through (Figure 24). From the design presented in the literature [11] it is known that only one inlet per solution was used, in a square surface of 10*10 cm^2 of effective area. This leads to a diagonal solution path, it is not clarified if all the membrane area was covered.

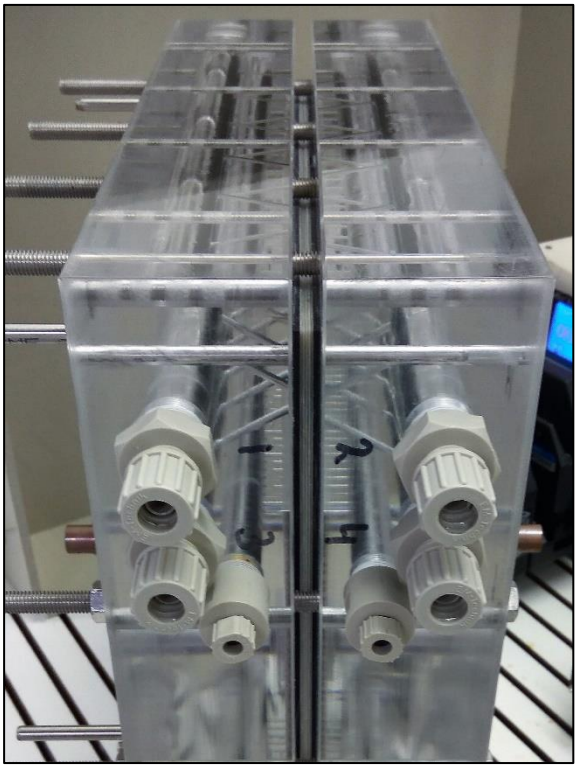

Figure 22 - Design 2 with 5 distributors.

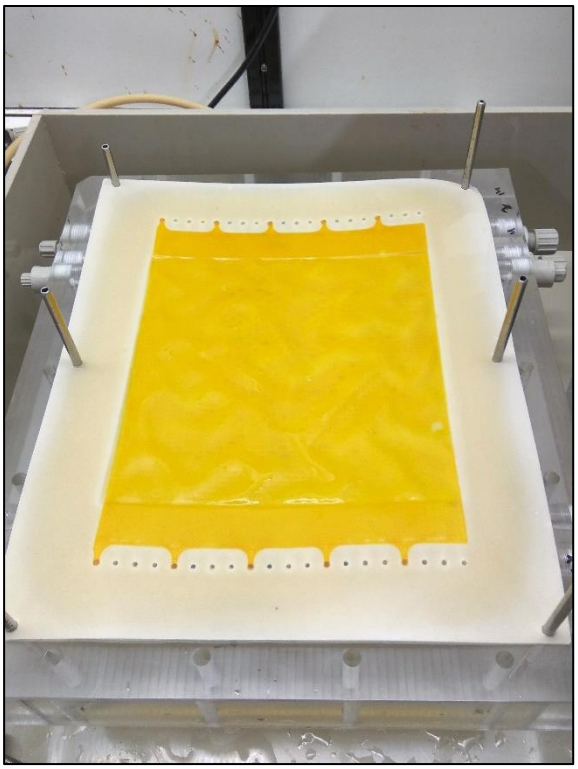

Figure 23 - Flow distribution in design 2.

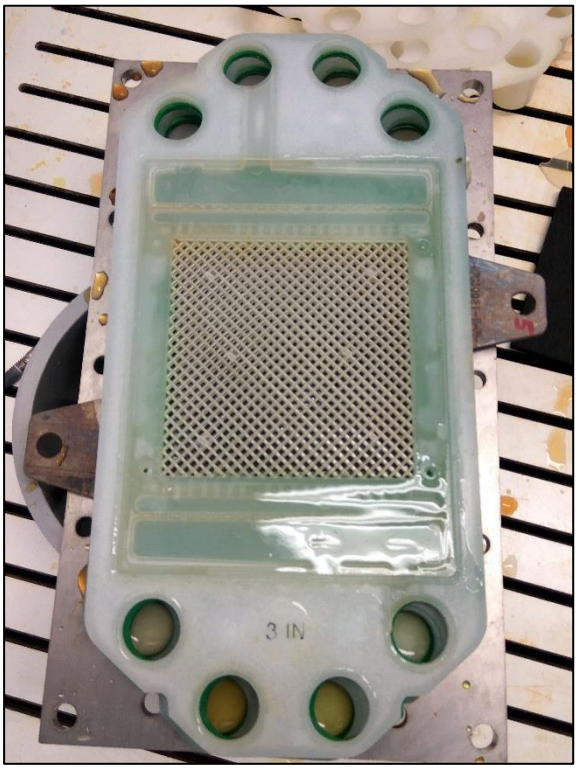

Figure 24 - Spacer of design 3 which assures the flow distribution.

In the present work the starting point studied was different from the considered cell design used in the previous literature. As referred in the methods section, for design 2 and 3 the stack used a charged state (100 % SOC) whereas in literature it started from discharged state (0% SOC).

Figure 25 shows the best coulombic efficiency and the round-trip efficiency achieved for each different design.

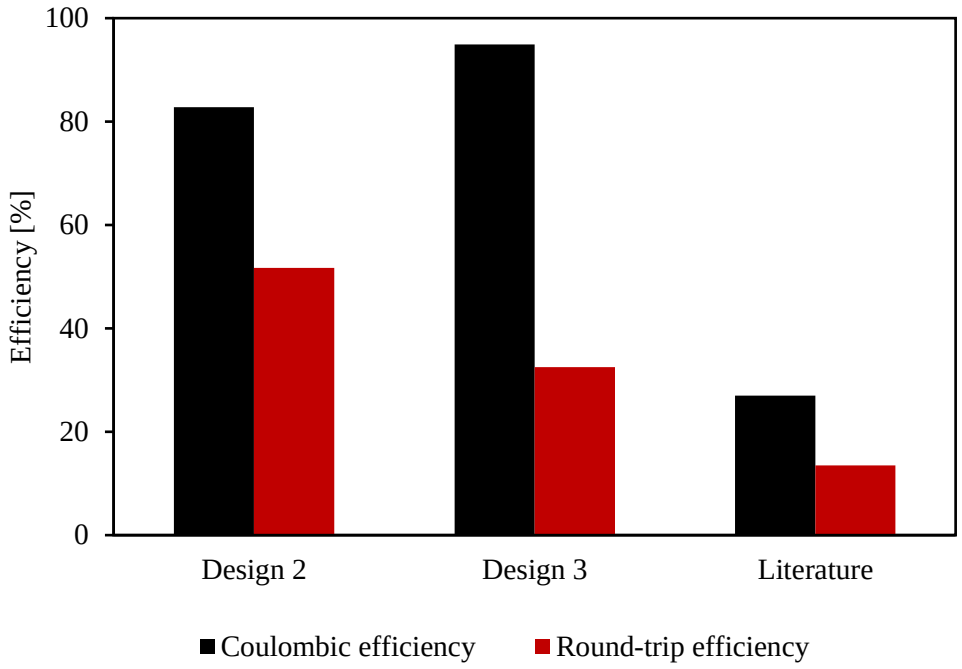

Figure 25- Coulombic efficiency (η_{CE}) and round-trip efficiency (η_{RTE}) from design 2, design 3 and literature [11]. The best value of round-trip efficiency from design 2 and for the literature were chosen, then design 3 was chosen based on the same current density of charge and discharge from design 2. The coulombic efficiency was the respective to each experiment. The highest round-trip efficiency obtained was 51.7%. The highest coulombic efficiency obtained was 94.9%.

	Design 2	**Design 3**	**Literature** [11]
i_{Charge} **[A m^{-2}]**	50	50	100
$i_{Discharge}$ **[A m^{-2}]**	37.5	37.5	15

The coulombic and round-trip efficiency of the experimental work were much higher than reached in the literature, as Figure 25 demonstrates. Many factors may explain the improvement. First the different starting point. In this study the start was done with acid and base solutions, avoiding the presence of co-ions in the acid and base compartments. The current density used for discharge was more than doubled, at higher current densities the contact time of the solutions is shortened. The homogeneous flow distribution is crucial to ensure the use of the complete membrane area, and by that the current density is homogenised over the membrane. Change of the redox solution and the electrode material (Pt coated Ti

mesh with 1 or 2 layers of graphite felt), and consequently the configuration of the membranes also had a positive influence. Chemically resistant gaskets and spacers materials were used to prevent internal leakages.

The excellent sealing of design 3 is the reason for its high coulombic efficiency of 94.9 %, while design 2 only reaches 82.8 %. Therefore, there is still opportunity to improve design 2 sealing using a fluoro-elastomeric type sealing. Efforts in this direction will be started. Round-trip efficiency is higher with design 2 compared with design 3, which can be explained due difference of the compartments thickness, while with design 2 a 0.5 mm thickness is used, design 3 uses a 7 mm thickness which creates higher resistance in the compartments resulting in higher voltage losses there.

Scaling up (design 2) shows improvement in the results compared to the smaller stacks, also because of the different materials/conditions used. It also demonstrates scaling up is possible, although it was noticed that sealing and membrane assembly were more difficult to overcome.

To get the maximum power density, two approaches were used. First by using equation 16 (chapter 2.6.7.). Design 2 value was 18.7 Wm^{-2} (OCV = 0.792 V, R = 0.07 Ω and A = 0.04 m^2) and design 3 value was 7.5 Wm^{-2} (OCV = 0.783 V, R = 0.68 Ω and A = 0.01 m^2).

The second approach was by making the IV curve. Figure 26 and Figure 27 show the IV curve and the power density curve for design 2.

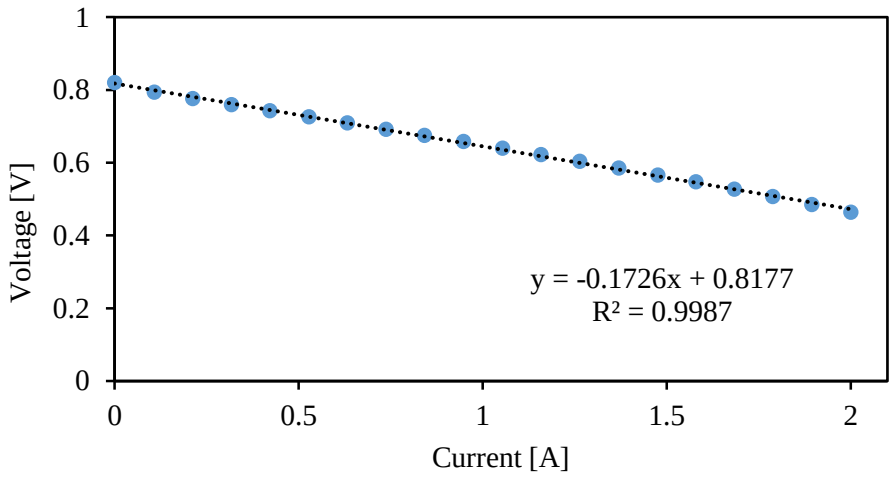

Figure 26 - IV curve for design 2. Higher current was not possible to apply due to instrument limitation.

The slope of the plot in Figure 26 represents the stack resistance and it is equal to 0.17 Ω and the OCV is 0.8177 V. From this plot, the power density curve can be achieved.

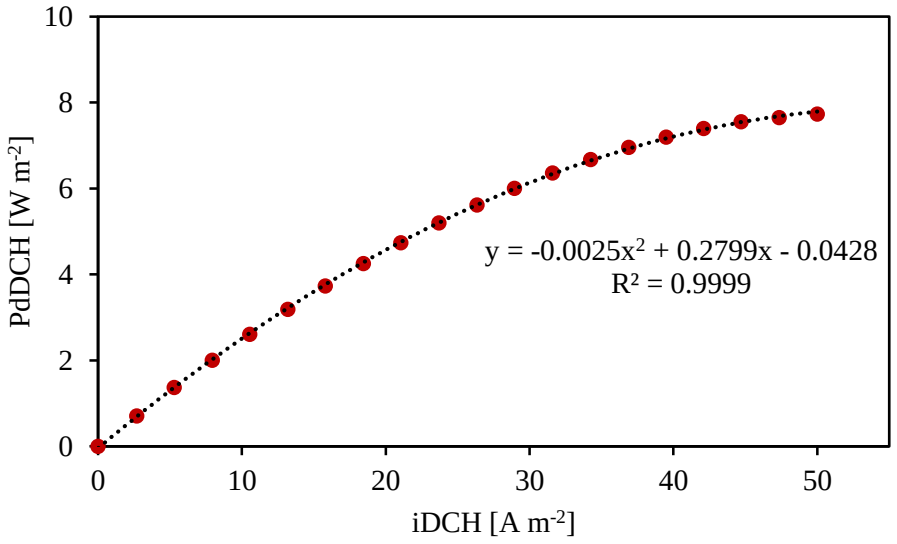

Figure 27 - Power density over the discharge current density for design 2.

By deriving equation present in Figure 27, and equalizing $\frac{dy\prime}{dx}$ to zero, which corresponds to the maximum of the parabola, the value for maximum power density is 7.9 Wm^{-2}. The associated current density is 56 Am^{-2}. Using the resistance and OCV values from Figure 26 with equation 16 (chapter 2.6.7.) the maximum power density value is 8.1 Wm^{-2}.

There is a difference of 10 Wm^{-2} between approaches. Although the conditions were the same, both experiments were independent, and the resistance calculation was made in different ways. First was by the difference in voltage from the OCV to discharge, and in the second it was the slope of the IV curve. Another IV curve should be made as confirmation since the value difference is significant.

For design 3, the same was made. Figure 28 and Figure 29 show the IV curve and the power density curve, respectively, for design 3.

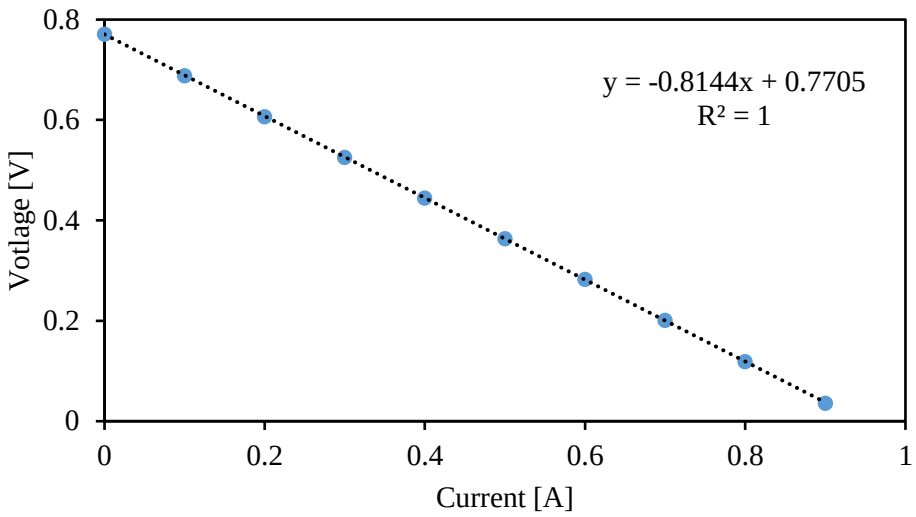

Figure 28 - IV curve for design 3.

The slope of the plot in Figure 28 represents the stack resistance and it is equal to 0.81 Ω and the OCV is 0.7705 V. From this plot, the power density curve can be achieved.

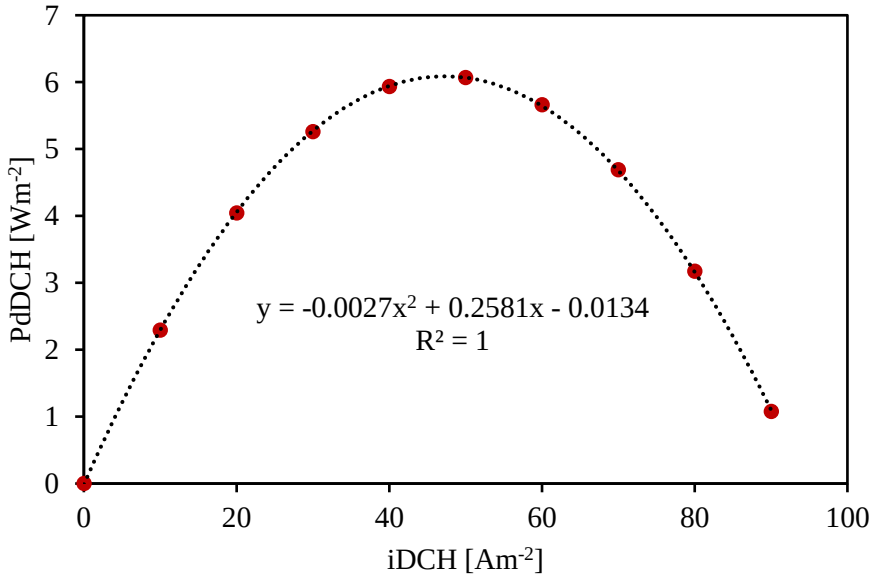

Figure 29 - Power density over the discharge current density for design 3.

The maximum power density is 6.2 Wm^{-2} and the maximum current density is 48 Am^{-2}. Using the resistance and OCV values from Figure 28 with equation 16 (chapter 2.6.7.) the maximum power density value is 6.1 Wm^{-2}.

Contrarily to design 2, the approaches have closer values. Again, the conditions were the same, but the experiments were independent, meaning not performed in the same day and other experiments were conducted in-between.

Regarding literature the value for maximum power density reported was 3.7 Wm^{-2} [11]. New designs show at least two times higher power density.

The energy density for design 2 was 1.5 WhL^{-1}, almost half of the theoretical value of 3.5 WhL^{-1} calculated in 2.6.5. The energy density in literature was 2.9 WhL^{-1}, higher than design 2, yet in this case the solutions were 1 M, and the theoretical energy density was 11 WhL^{-1}, referred in the article [11]. Experiments with design 2 and 3 using 1 M of HCl and 1 M of NaOH should be conducted, for a more accurate comparison.

4.5. Relation between Coulombic efficiency and co-ion loss

Co-ion transportation is one of the main challenges to overcome in order to achieve higher coulombic efficiencies and higher battery performance. Here is discussed a theory of a relation between the Coulombic efficiency and co-ion loss.

During charge of the AB-FB there is loss of charge due to co-ion transportation. Specifically, the transport of Na^+ and Cl^- (also called salt transport loss) through the BPM, as shown in chapter 4.3. This can be described by:

$$Q_{H_2O,dissociation} = Q_{CH,applied} - Q_{co-ion} \quad \text{Equation 17}$$

Where $Q_{CH,applied}$ is the charge, in Coulomb, applied to the cell by an external power supply and Q_{co-ion} is the loss of charge capacity by diffusion of co-ions (Na^+ and Cl^-) through the BPM. $Q_{H_2O,dissociation}$ is the actual true charge capacity for the formation of H^+ and OH^- and is referred as $Q_{CH,true}$.

$$Q_{CH,true} = Q_{CH,applied} - Q_{co-ion} \quad \text{Equation 18}$$

During discharge a loss is considered due to co-ion transport of Na^+ and Cl^- ions through the BPM. As a parallel process H^+ and OH^- diffuse to the junction of the BPM and form water. Therefore, the following relation is found:

$$Q_{DCH,true} = Q_{CH,true} - Q_{co-ion} \quad \text{Equation 19}$$

Where $Q_{DCH,true}$ is the discharge capacity as measured and Q_{co-ion} is the loss of discharge capacity by diffusion of co-ions (Na^+ and Cl^-) through the BPM.

The Coulombic efficiency can be theoretically calculated realizing that,

$$\eta_{CE} = \frac{Q_{DCH,true}}{Q_{CH,true}} = \frac{Q_{CH,true} - Q_{co-ion}}{Q_{CH,applied} - Q_{co-ion}} = \frac{Q_{CH,applied} - Q_{co-ion} - Q_{co-ion}}{Q_{CH,applied} - Q_{co-ion}} \quad \text{Equation 20}$$

Since Q_{co-ion} is a fraction of the charge applied, it can be introduced as $Q_{co-ion} = f.Q_{CH,applied}$ with f is a value between 0 and 1.

By making the substitution in equation 20:

$$\eta_{CE} = \frac{Q_{CH,applied} - 2Q_{co-ion}}{Q_{CH,applied} - Q_{co-ion}} = \frac{Q_{CH,applied}\,(1-2f)}{Q_{CH,applied}\,(1-f)} = \frac{1-2f}{1-f} \qquad \text{Equation 21}$$

Where η_{CE} is a value between 0 and 1 and f is the fraction of the charge applied that is lost to co-ion transport. The fraction lost, given by f, can be calculated from equation 21 by rearranging it:

$$f = \frac{\eta_{CE} - 1}{\eta_{CE} - 2} \qquad \text{Equation 22}$$

With equation 21 the Coulombic efficiency can be plotted as a function of f, represented in Figure 30.

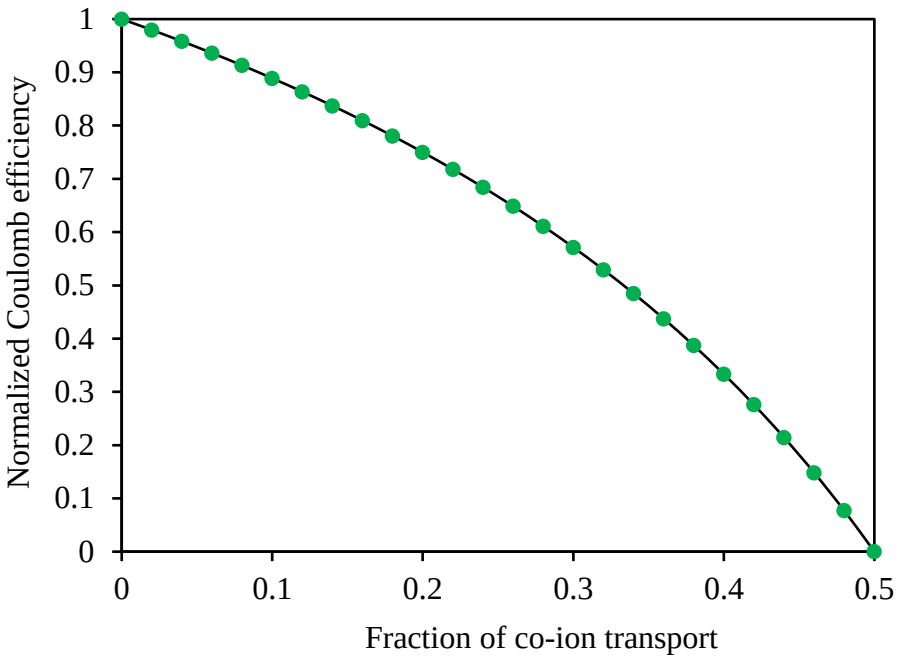

Figure 30 - Coulombic efficiency (normalized to 1) versus fraction of loss by co-ion transport.

If $f = 0.5$ the Coulombic efficiency goes to zero, meaning that during charge half of the charge is lost due to co-ion transport and that during discharge the other half is lost due to co-ion transport as well. The result is zero net to discharge.

In order to get a Coulombic efficiency larger than 0.95 (95 %), we need a value of f that is smaller than 0.047, which means the loss due to co-ion transport must be less than 4.7 %. Considering no other factors are affecting the coulombic efficiency.

5. Conclusion

In the present work new stack designs were developed and tested to improve the AF-FB as a suitable EES system.

With **design 1** a reduction of 60 % in the resistance of the electrodes was achieved by adding one layer of graphite felt at the electrodes. Due to internal leakage and due to poor material properties of the 500 µm silicone rubber no more experiments were conducted with this design. The graphite felt was applied to the other designs.

Design 2 was used to study round-trip efficiency at different current densities for charging and discharging. The best round-trip efficiency was 51.7 %, by this the goal of surpassing 50 % was achieved. The coulombic efficiencies were quite high (75 % – 83 %). It was concluded with this experiment that high current densities provide better coulombic and round-trip efficiencies. Due to the potentiostat limitation (2A) higher current densities were not tested. Nonetheless, improvement in the membranes selectivity should reduce co-ion transportation and so even higher values can be attained. Furthermore, this design is a first scale-up to 400cm^2 of previous studies (100cm^2), showing that scale-up is possible and the properties can be improved.

Finally, **design 3** proved that cycling with the AB-FB is feasible. Once more the need of better membrane selectivity is the key to improve further. Importantly, after 10 cycles the battery performance was maintained with slight decrease of the round trip efficiency. The coulombic efficiency has a 1 % fading rate over each cycle while the round-trip efficiency has a 0.4 % fading rate over each cycle. The low round-trip efficiency (20 % - 16%) was caused mainly by the large compartment thickness (7 mm), which increased the resistance. Very high coulombic efficiencies (94 % - 84 %) were reached because of good sealing material made of fluoro-elastomeric rubber sheets, the sealing ridge technology used and the very uniform flow inside the cell.

By developing new cell designs with equal distribution of the solutions inside the cell, applying graphite felt at the electrodes to lower the electrode losses, studying at a better starting point (0.5 M acid and base solutions) than in previous literature (1.0 M acid and base solutions) to have less co-ion transport of protons, and applying chemically stable sealing technology the round-trip efficiency increased from 13.5 % [11] to 51.7 %. The energy density reached (1.5 WhL^{-1}) was almost half of the theoretical (3.5 WhL^{-1}).

Although future investigation is still needed, the work performed in the frame of this Master thesis project clearly shows strong improvements in the AB-FB performance and puts it closer to compete with other EES. The environmental benefits of the system developed, and its potential are the stimulus to convert it into a mature technology. The required future target is a round-trip efficiency of at least

70% to compete with existing technologies like all-vanadium, all iron, hydrogen-bromine and zinc-bromine redox flow batteries.

6. Future recommendations

In further investigations the following advices should be considered:

- A bipolar membrane that allows higher discharge current densities is needed, to avoid ballooning/delamination.
- The proton blocking properties of the anion exchange membrane need to be further improved.
- Test of different solution concentrations.
- For design 3 (ElectroCell) the use of an ion exchange resin in the salt compartment can lower the cell resistance drastically, thus improving the performance [52].
- The number of cycles need to be extended to 100 or more.
- Deep discharge and charge need to be avoided to improve the round-trip efficiency.
- The round-trip efficiency of design 2 (large stack, 400cm^2) needs to be improved using fluoroelastomeric sealing technology being chemical stable in contact with strong acids and strong bases [53]. This path line is under development.
- The use of online pH and conductivity measurements needs to be considered to evaluate in more detail the process and to derive conditions for improved round-trip efficiency.
- The use of more than one cell pair needs to be tested to investigate the effect of stacking.
- Monitoring with two reference electrodes the BPM voltage (like Ag, AgCl) to control if the charge current density is high enough to support water dissociation. In this way unwanted transport of Na^+ and Cl^- through the BPM can be prevented.
- Charge at higher current density to have less co-ion transport of Na^+ and Cl^- during charging.

References

[1] Eurostat, Renewable energy produced in the EU increased by two thirds in 2006-2016, (2018). http://ec.europa.eu/eurostat/statistics-explained/index.php/Renewable_energy_statistics#Renewable_energy_produced_in_the_EU_increased_by_two_thirds_in_2006-2016.

[2] W. He, J. Wang, Feasibility study of energy storage by concentrating/desalinating water: Concentrated Water Energy Storage, Appl. Energy. 185 (2017) 872–884. doi:10.1016/j.apenergy.2016.10.077.

[3] International Renewable Energy Agency, Electricity Storage and Renewables : Costs and Markets To 2030, 2017.

[4] R.S. Kingsbury, K. Chu, O. Coronell, Energy storage by reversible electrodialysis: The concentration battery, J. Memb. Sci. 495 (2015) 502–516. doi:10.1016/j.memsci.2015.06.050.

[5] B.E. Logan, M. Elimelech, Membrane-based processes for sustainable power generation using water, Nature. 488 (2012) 313–319. doi:10.1038/nature11477.

[6] Z. Jia, B. Wang, S. Song, Y. Fan, Blue energy: Current technologies for sustainable power generation from water salinity gradient, Renew. Sustain. Energy Rev. 31 (2014) 91–100. doi:10.1016/j.rser.2013.11.049.

[7] J.N. Weinstein, F.B. Leitz, Electric power from differences in salinity: the dialytic battery, Science. 191 (1976) 557–559. doi:10.1126/science.191.4227.557.

[8] G.L. Wick, Power from salinity gradients, Energy. 3 (1978) 95–100. doi:10.1016/0360-5442(78)90059-2.

[9] R.E. Lacey, Energy by reverse electrodialysis, Ocean Eng. 7 (1980) 1–47. doi:10.1016/0029-8018(80)90030-X.

[10] W.J. van Egmond, M. Saakes, S. Porada, T. Meuwissen, C.J.N. Buisman, H.V.M. Hamelers, The concentration gradient flow battery as electricity storage system: Technology potential and energy dissipation, J. Power Sources. 325 (2016) 129–139. doi:10.1016/j.jpowsour.2016.05.130.

[11] W.J. van Egmond, M. Saakes, I. Noor, S. Porada, C.J.N. Buisman, H.V.M. Hamelers, Performance of an environmentally benign acid base flow battery at high energy density, Int. J. Energy Res. (2017) 1–12. doi:10.1002/er.3941.

[12] A.T. Emrén, V.J.M. Holmström, Energy storage in a fuel cell with bipolar membranes burning

acid and hydroxide, Energy. 8 (1983) 277–282. doi:10.1016/0360-5442(83)90103-2.

[13] E.K. Zholkovskij, M.C. Müller, E. Staude, The storage battery with bipolar membranes, J. Memb. Sci. 141 (1998) 231–243. doi:10.1016/S0376-7388(97)00306-2.

[14] J. Pretz, E. Staude, Reverse Electrodialysis (RED) with Bipolar Membranes, and Energy Storage System, Berichte Der Bunsengesellschaft Für Phys. Chemie. (1998) 676–685.

[15] J.H. Kim, J.H. Lee, S. Maurya, S.H. Shin, J.Y. Lee, I.S. Chang, S.H. Moon, Proof-of-concept experiments of an acid-base junction flow battery by reverse bipolar electrodialysis for an energy conversion system, Electrochem. Commun. 72 (2016) 157–161. doi:10.1016/j.elecom.2016.09.025.

[16] G. Wetstone, K. Thornton, R. Hinrichs-rahlwes, S. Sawyer, M. Sander, R. Taylor, D. Rodgers, M. Alers, H. Lehmann, M. Eckhart, D. Hales, Renewables 2016 global status report 2016, 2016.

[17] C. Gissey, G. Dodds, P. E., J. Radcliffe, Market and regulatory barriers to electrical energy storage innovation, Renew. Sustain. Energy Rev. 82 (2018) 781–790. doi:10.1016/j.rser.2017.09.079.

[18] X. Luo, J. Wang, M. Dooner, J. Clarke, Overview of current development in electrical energy storage technologies and the application potential in power system operation, Appl. Energy. 137 (2015) 511–536. doi:10.1016/j.apenergy.2014.09.081.

[19] C. Zhang, Y.L. Wei, P.F. Cao, M.C. Lin, Energy storage system: Current studies on batteries and power condition system, Renew. Sustain. Energy Rev. 82 (2018) 3091–3106. doi:10.1016/j.rser.2017.10.030.

[20] C.J. Rydh, Environmental assessment of vanadium redox and lead-acid batteries for stationary energy storage, J. Power Sources. 80 (1999) 21–29. doi:10.1016/S0378-7753(98)00249-3.

[21] L.W. Hruska, Investigation of Factors Affecting Performance of the Iron-Redox Battery, J. Electrochem. Soc. 128 (1981) 18. doi:10.1149/1.2127366.

[22] K.L. Hawthorne, J.S. Wainright, R.F. Savinell, Studies of Iron-Ligand Complexes for an All-Iron Flow Battery Application, J. Electrochem. Soc. 161 (2014) A1662–A1671. doi:10.1149/2.0761410jes.

[23] ESS Technical White Paper: All-Iron Flow Battery, (2016).

[24] S. Hameer, J.L. van Niekerk, A review of large-scale electrical energy storage, Int. J. Energy Res. 39 (2015) 1179–1195. doi:10.1002/er.3294.

[25] World Energy Council, World Energy Resources - E-Storage, World Energy Counc. Rep. 1 (2016) 60. doi:http://www.worldenergy.org/wp-content/uploads/2013/09/Complete_WER_2013_Survey.pdf.

[26] H. Chen, T.N. Cong, W. Yang, C. Tan, Y. Li, Y. Ding, Progress in electrical energy storage system: A critical review, Prog. Nat. Sci. 19 (2009) 291–312. doi:10.1016/j.pnsc.2008.07.014.

[27] A. Chatzivasileiadi, E. Ampatzi, I. Knight, Characteristics of electrical energy storage technologies and their applications in buildings, Renew. Sustain. Energy Rev. 25 (2013) 814–830. doi:10.1016/j.rser.2013.05.023.

[28] W.J. van Egmond, U.K. Starke, M. Saakes, C.J.N. Buisman, H.V.M. Hamelers, Energy efficiency of a concentration gradient flow battery at elevated temperatures, J. Power Sources. 340 (2017) 71–79. doi:10.1016/j.jpowsour.2016.11.043.

[29] G.H. Brundtland, Our Common Future: Report of the World Commission on Environment and Development, United Nations Comm. 4 (1987) 300. doi:10.1080/07488008808408783.

[30] T. Sata, Ion Exchange Membranes: Preparation, Characterization, Modification and Application, 2004. doi:10.1039/9781847551177.

[31] H. Strathmann, H.J. Rapp, B. Bauer, C.M. Bell, Theoretical and practical aspects of preparing bipolar membranes, Desalination. 90 (1993) 303–323. doi:10.1016/0011-9164(93)80183-N.

[32] F.G. Wilhelm, Bipolar Membrane Electrodialysis - Membrane Development and Transport Characteristics, 2001. doi:10.1016/S0927-5193(07)12017-9.

[33] C. Huang, T. Xu, Electrodialysis with bipolar membranes for sustainable development, Environ. Sci. Technol. 40 (2006) 5233–5243. doi:10.1021/es060039p.

[34] S. Sridhar, Electrodialysis in a non-aqueous medium: Production of sodium methoxide, J. Memb. Sci. 113 (1996) 73–79. doi:10.1016/0376-7388(95)00217-0.

[35] A.J.B. Kemperman, Handbook Bipolar Membrane Technology, Twente University Press, Enschede, 2000.

[36] H. Strathmann, J.J. Krol, H.J. Rapp, G. Eigenberger, Limiting current density and water dissociation in bipolar membranes, J. Memb. Sci. 125 (1997) 123–142. doi:10.1016/S0376-7388(96)00185-8.

[37] C. Shen, R. Wycisk, P.N. Pintauro, High performance electrospun bipolar membrane with a 3D junction, Energy Environ. Sci. 10 (2017) 1435–1442. doi:10.1039/c7ee00345e.

[38] R. Simons, Preparation of a high performance bipolar membrane, J. Memb. Sci. 78 (1993) 13–23. doi:10.1016/0376-7388(93)85243-P.

[39] J. Pan, L. Hou, Q. Wang, Y. He, L. Wu, A.N. Mondal, T. Xu, Preparation of bipolar membranes by electrospinning, Mater. Chem. Phys. 186 (2016) 484–491. doi:10.1016/j.matchemphys.2016.11.023.

[40] H. Strathmann, Ion-Exchange Membrane Separation Processes, 2004. doi:10.1007/s13398-014-0173-7.2.

[41] H. Strathmann, Electrodialysis, a mature technology with a multitude of new applications, Desalination. 264 (2010) 268–288. doi:10.1016/j.desal.2010.04.069.

[42] J.W. Post, J. Veerman, H.V.M. Hamelers, G.J.W. Euverink, S.J. Metz, K. Nymeijer, C.J.N. Buisman, Salinity-gradient power: Evaluation of pressure-retarded osmosis and reverse electrodialysis, J. Memb. Sci. 288 (2007) 218–230. doi:10.1016/j.memsci.2006.11.018.

[43] F.L. Ramp, Secondary batteries powered by forced ionisation, Nature. (1979) 335–337.

[44] J.F. Walther, Process for Production of Electrical Energy from the Neutralization of Acid and Base in a Bipolar Membrane Cell, 1982.

[45] M. Ulaganathan, A. Jain, V. Aravindan, S. Jayaraman, W.C. Ling, T.M. Lim, M.P. Srinivasan, Q. Yan, S. Madhavi, Bio-mass derived mesoporous carbon as superior electrode in all vanadium redox flow battery with multicouple reactions, J. Power Sources. 274 (2015) 846–850. doi:10.1016/j.jpowsour.2014.10.176.

[46] W.J. Saakes, M., Hamelers, H.V.M., van Egmond, Method for Operating of a Regenerative Bipolar Membrane Fuel Cell, and Regenerative Bipolar Membrane Fuel Cell There For, 2018.

[47] P. Dlugolecki, K. Nymeijer, S. Metz, M. Wessling, Current status of ion exchange membranes for power generation from salinity gradients, J. Memb. Sci. 319 (2008) 214–222. doi:10.1016/j.memsci.2008.03.037.

[48] Fumatech, f u m a s e p ® F K B - P K - 1 3 0. http://www.fuelcellstore.com/spec-sheets/fumasep-fkb-pk-130-technical-specifications.pdf (27/03/2018)

[49] Fumatech, f u m a s e p ® F A B - P K - 1 3 0. http://www.fuelcellstore.com/spec-sheets/fumasep-fab-pk-130-technical-specifications.pdf (27/03/2018)

[50] Fumatech, fumasep® FBM Technical Data Sheet. http://www.fuelcellstore.com/spec-sheets/fumasep-fbm-pk-technical-specifications.pdf (27/03/2018)

[51] J. Veerman, M. Saakes, S.J. Metz, G.J. Harmsen, Reverse electrodialysis: Evaluation of suitable electrode systems, J. Appl. Electrochem. 40 (2010) 1461–1474. doi:10.1007/s10800-010-0124-8.

[52] H. Yang, J.J. Kaczur, S.D. Sajjad, R.I. Masel, Electrochemical conversion of CO2 to formic acid utilizing Sustainion™ membranes, J. CO2 Util. 20 (2017) 208–217. doi:10.1016/j.jcou.2017.04.011.

[53] B. Améduri, B. Boutevin, G. Kostov, Fluoroelastomers: synthesis, properties and applications, Prog. Polym. Sci. 26 (2001) 105–187. doi:10.1016/S0079-6700(00)00044-7.

Appendix A – Designs Set-ups and Leakage Problems

Design 1: Wetsus cell design with 400cm^2 electrode surface.

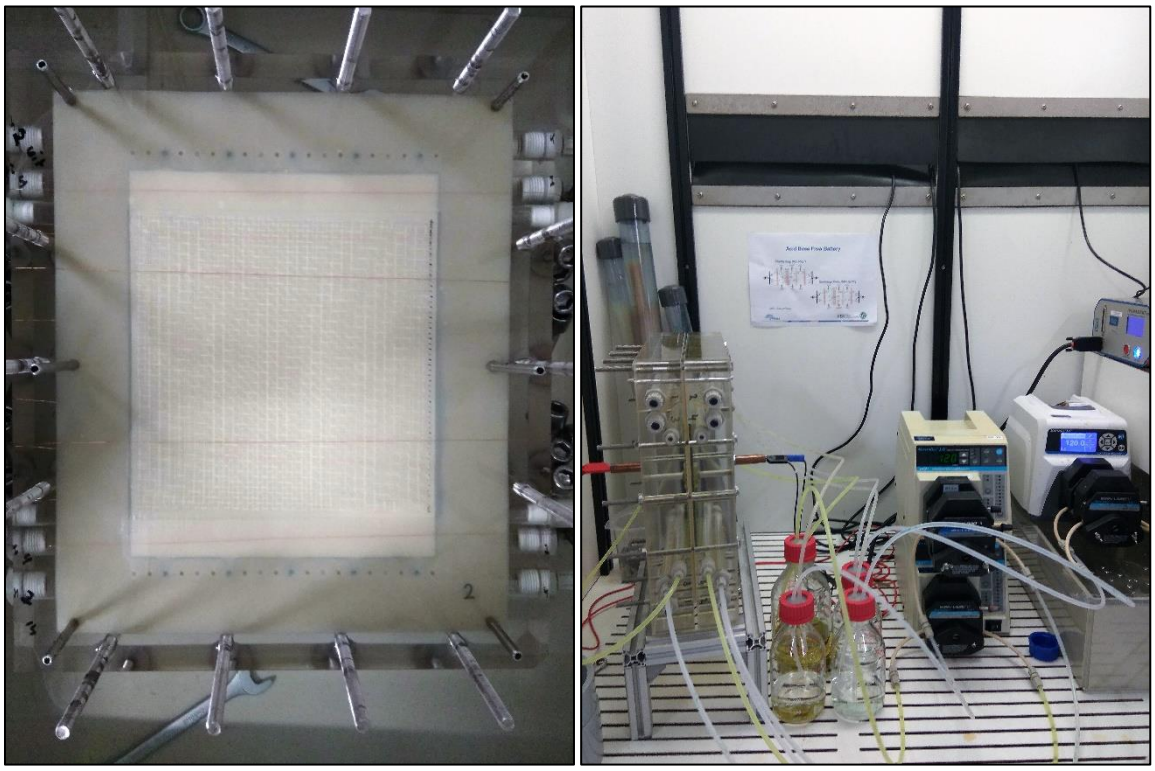

Design 2: Wetsus cell design (AQUASEAL) with 400cm^2 electrode surface.

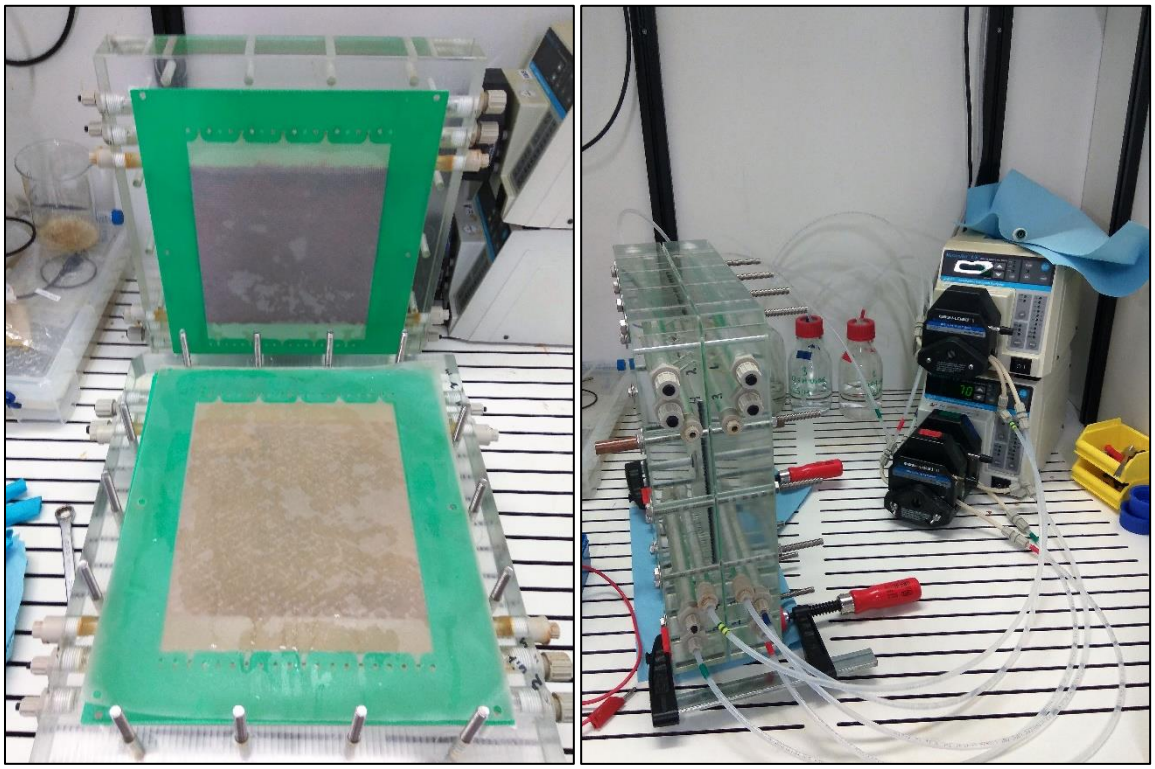

Design 3: ElectroCell Design with 100cm^2 electrode surface.

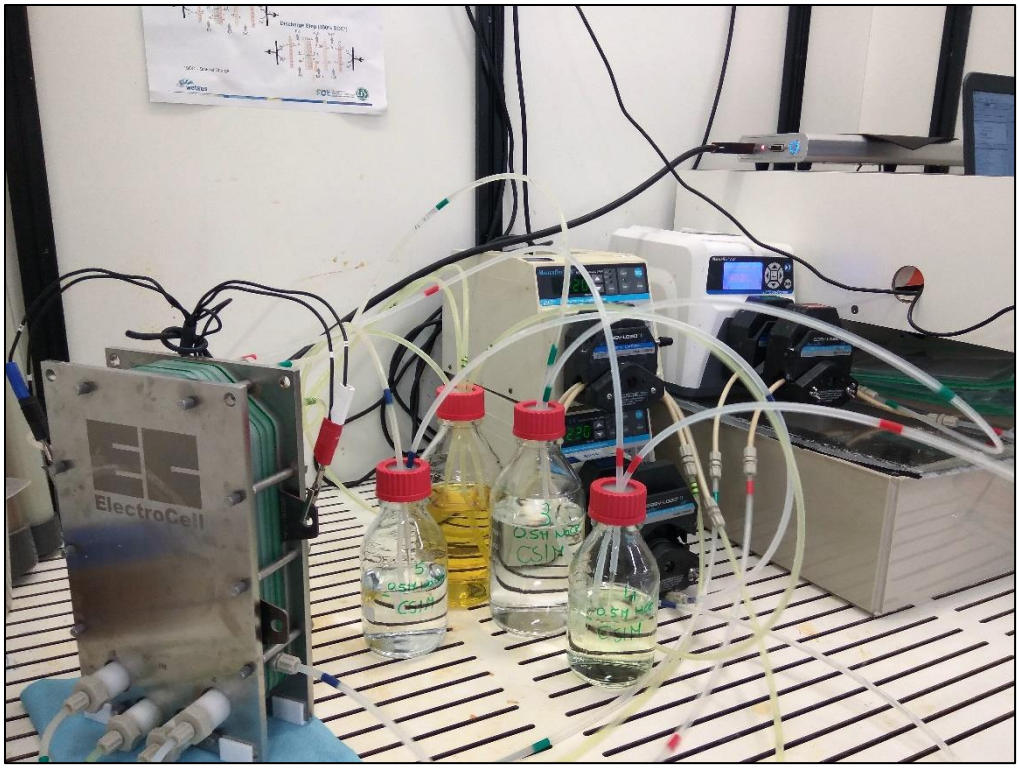

Leakage trouble design 1: due to thickness variations in 0.5mm silicone rubber.

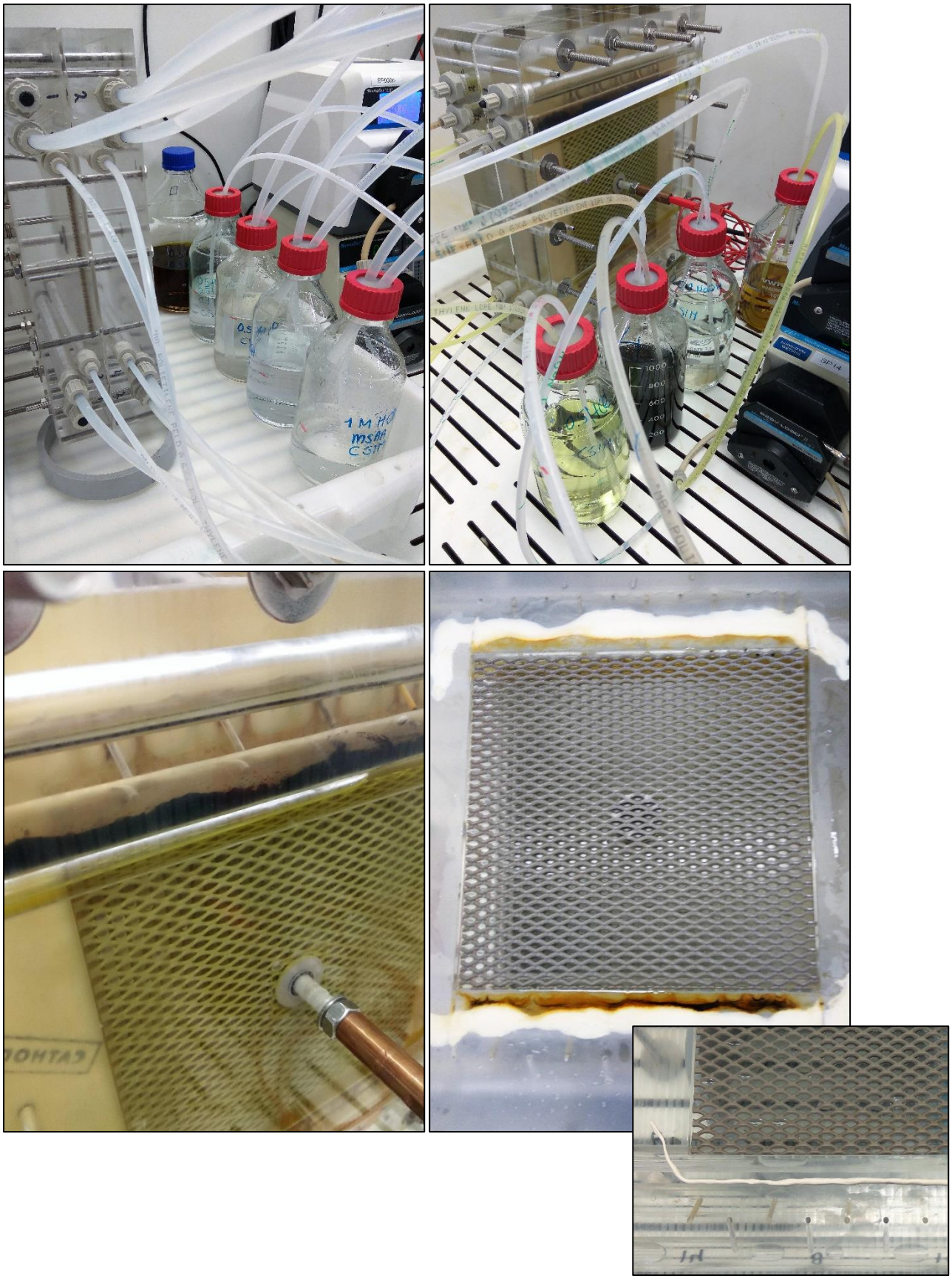

Appendix B – Data for Resistance of the electrodes (design 1)

Table 10 - Average resistance for each case in Ω and Ωcm²

	Without graphite felt	With graphite felt
Resistance [Ω]	0.193	0.058
	0.200	0.068
	0.130	0.071
		0.078
Average	0.175	0.069
Average [Ωcm²]	69.789	27.511

Appendix C – Data of design 2 at different current densities

Table 11 - Coulombic efficiency, round-trip efficiency and resistance of design 2 experiments

	$i_{CH} - i_{DCH}$ [Am^{-2}]	Coulombic Efficiency (%)	Round-trip efficiency (%)	Resistance [Ωcm^2]	Date
1	25 - 25	74.9	51.7	39.4	21.07
2	37.5 – 37.5	77.2	39.1	38.6	24.07
3	37.5 - 50	76.2	43.9	38.5	26.07
4	50 – 37.5	82.7	**51.7**	28.7	19.07
5	50 – 50	82.8	46.0	31.1	19.07

Appendix D – Second experiment with design 3

Another experiment of cycling with design 3 was conducted.

Figure 31 shows the cell voltage of the stack during ten consecutive cycles. The experiment lasted around 7 days. The last cycle only charged, and discharge was not possible.

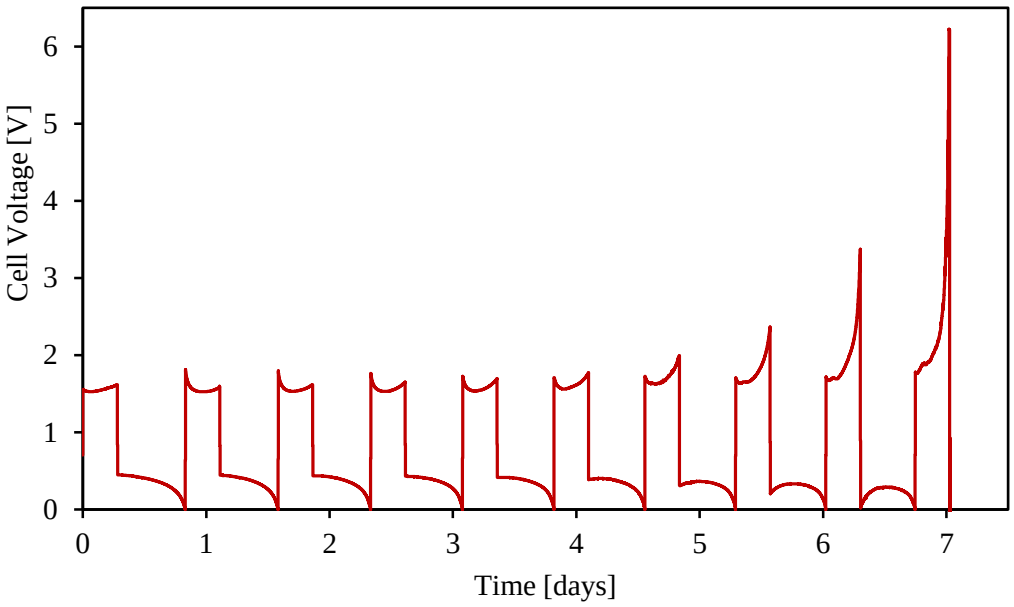

Figure 31 – Cell voltage over the experiment time.

In this case, from the first cycle to the final one, the differences are plain. Whilst in the beginning curves are similar and with longer times of discharge, when reaching the 7th cycle the behaviour changed. The reason for this to happen was a small external leakage in the salt compartment, because the Neoprene tubing got damaged by the high speed of the pump.

Figure 32 shows the cycles overlap, where the cell voltage, in Volts, is plotted versus the time, in hours.

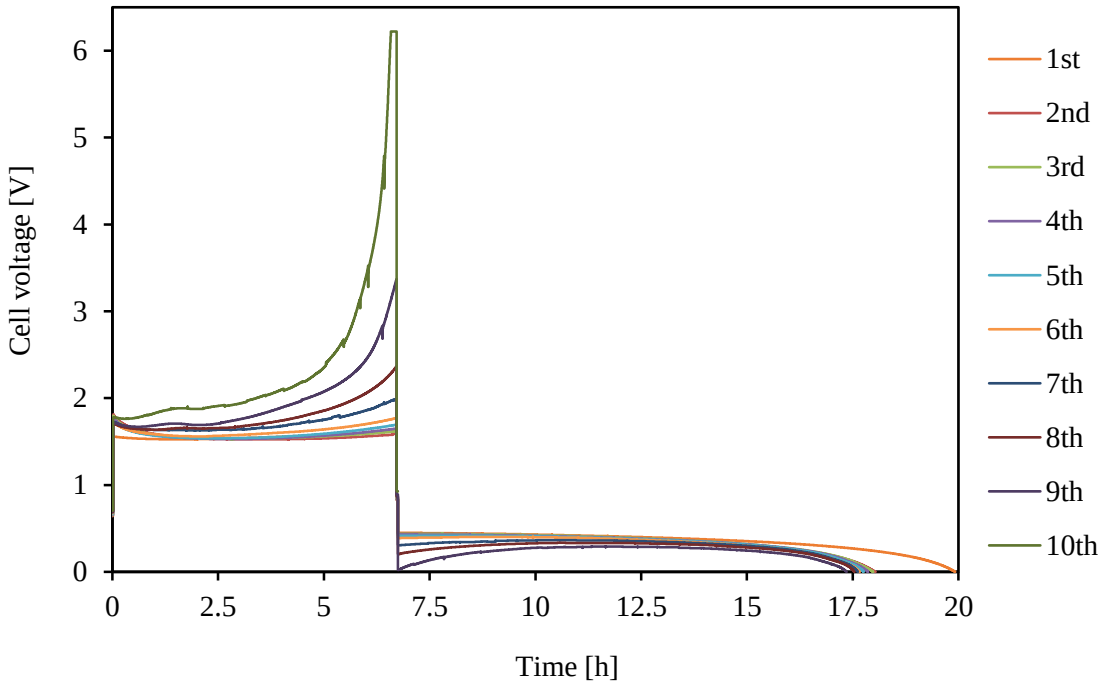

Figure 32 - Cycles overlap. First, charging with 100 A m^{-2} for 6.7 hours, followed by 1-minute OCV and discharging with 50 A m^{-2} until the potential reaches zero. The experiment was performed in continuous state (no interruptions between cycles).

The difference between cycles is evident in Figure 32 where the cycles overlap. The first cycle had 2.5 hours more of discharge than the following ones. Since a leakage in the salt tube was detected during the last cycles of the experiment, it is possible to see the effect it had on the cell voltage. The increased cell voltage at the end of charging is due to the fact that the salt compartment got every cycle more depleted of ions at the end of the charging process, lowering the conductivity in that compartment. With a lower conductivity it got more difficult for the current to pass. Until the 9^{th} cycle the battery was able to recover cell voltage and discharge. On that cycle when starting to discharge the cell voltage reached almost zero volt but the battery recovered (the line after the start of discharge goes up) due to the salt compartment gained conductivity again and ended up discharging normally. For the last cycle the salt solution got depleted and the compartment lost conductivity, so no discharge was possible.

In Table 12 is shown the initial (calculated) and final (through IC measurement) concentration of chloride and sodium in each compartment.

Table 12 - Chloride and sodium concentration before and after cycling in each compartment

Compartment	Ion	Initial concentration [M]	Final concentration [M]
Acid	Cl^-	0.5	0.70
	Na^+	0.0	**0.18**
Base	Cl^-	0.0	**0.12**
	Na^+	0.5	0.80
Salt	Cl^-	0.5	0.03
	Na^+	0.5	0.03
Redox	Cl^-	0.1	0.50
	Na^+	0.0	0.02

In this experiment the last discharge was not possible to do so the IC measurements correspond to the charged state. Which means concentrated acid and base, and diluted salt. Co-ion transportation of Na^+ and Cl^- is demonstrated in the acid and base compartment (Table 12 in **bold**). Only 0.03 M of Na^+ and Cl^- ion is present in the salt compartment, so the availability of ions to carry the current is very low.

The pH and conductivity of each compartment after cycling is measured and presented in Table 13. Note that that pH measurement of 0.5 M H^+ should read pH = 0.30 but this is outside the calibration range of the pH meter (calibrated at pH = 4). Same happens to the pH measurement of 0.5 M OH^-, it should read pH = 13.70 but this is outside the calibration range of the pH meter (calibrated at pH=10).

Table 13 - pH and conductivity after cycling for each compartment

Compartment	pH	Conductivity [mS/cm]
Acid	0.448	194.0
Base	13.439	130.0
Salt	2.581	42.8
Redox	0.681	86.5

Compared to the acid and base compartment the conductivity measured in the salt compartment is very low (around 4 times lower) and half of the redox compartment. It is possible the salt compartment re-stored some conductivity between the end of the experiment and the measurement moment, the pumps were manually stopped. The salt compartment has decreased in pH which indicates proton leakage.

Figure 33 represents the resistance of the stack over the cycles. It is calculated from the cell voltage drop at the start of discharge after one minute OCV through equation 13 (chapter 2.6.6.).

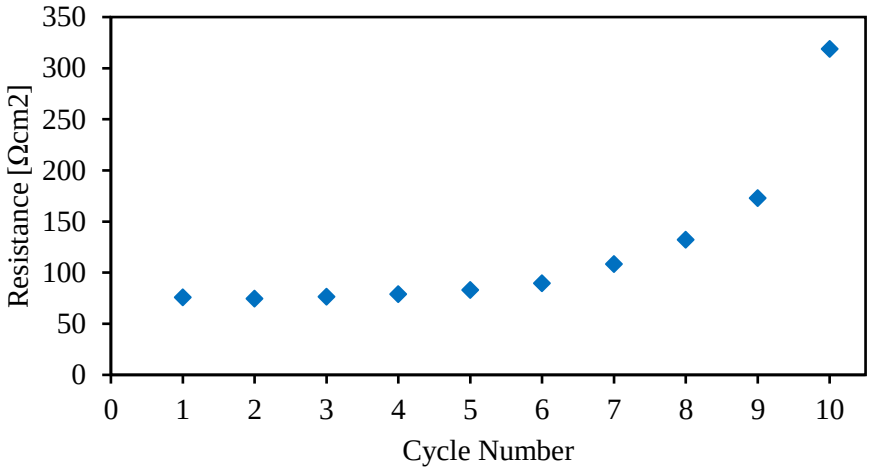

Figure 33- Stack resistance at the start of discharging in each cycle.

In Figure 33, the first cycle has the expected small increase in resistance due to the co-ion transportation, but from the 7th round the increase is notorious and the last cycle has around 7 times the resistance of the first one.

The coulombic efficiency (η_{CE}) and round-trip efficiency (η_{RTE}) are plotted in Figure 34. These parameters were calculated for each cycle, using equations 9 and 10, respectively.

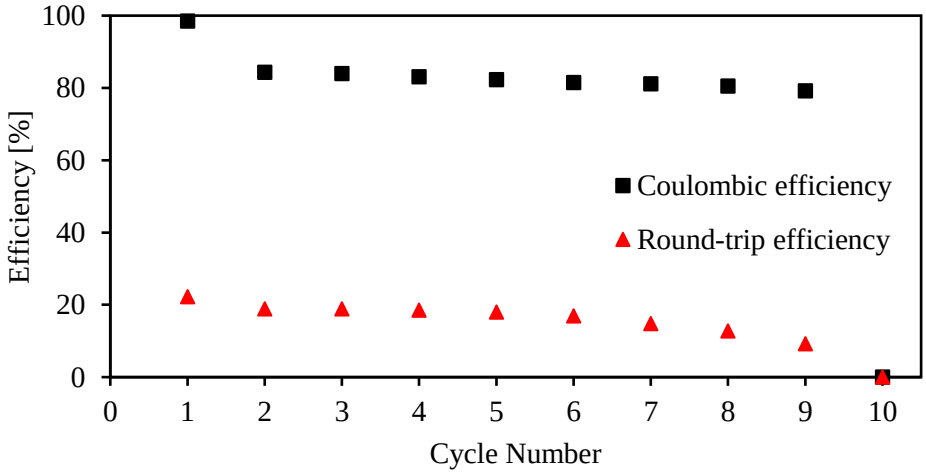

Figure 34 - Coulombic efficiency (η_{CE}) and round-trip efficiency (η_{RTE}) over 10 cycles. The current density of charging was 100 Am^{-2} and of discharging was 50 Am^{-2}.

Figure 35 focuses on the coulombic efficiency and round-trip efficiency from cycle 2 to 9, a tendency line is added to show the decrease in each efficiency.

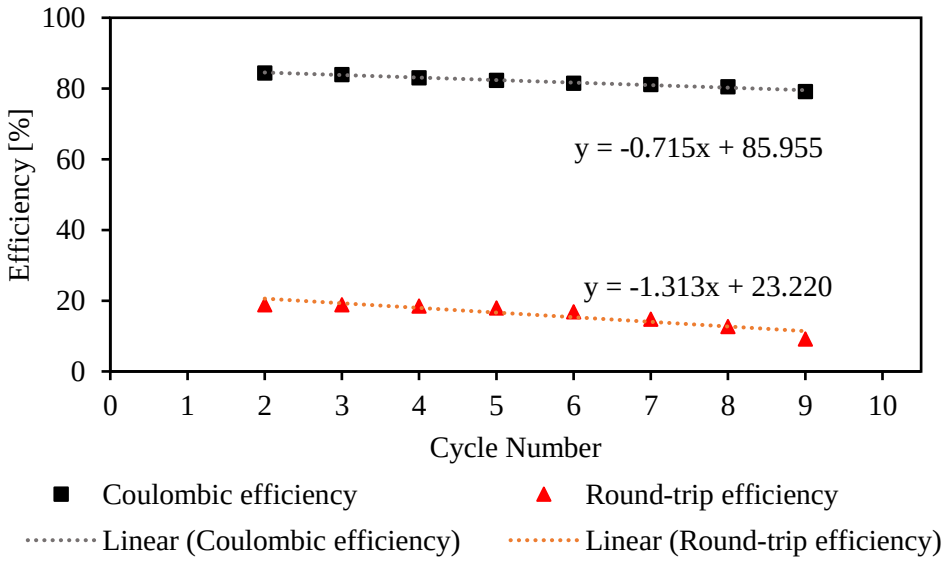

Figure 35 - Coulombic efficiency and round-trip efficiency from cycle 2 to 9.

The coulombic and round-trip efficiency in the first cycle were the highest reached with the design 3 (98.5% and 22.3%, respectively). The coulombic efficiency after the first cycle decreased 14% and remained after relatively stable since it decreased 5% in 8 cycles. The round-trip efficiency after the 7th cycle the performance decreased strongly due to the loss of salt solution due to the leaking Neoprene tubing as discovered later.

In Figure 35 by using a trending line from cycle 2 to 9, the fading rate was found. For the coulombic efficiency a fading rate of 0.7 % over each cycle occurs and for the round-trip efficiency a 1.3% fading rate over each cycle occurs. Despite the first and tenth cycle that show abnormalities regarding the pattern behaviour, the cycles between show stability until a certain point because of the leakage.

Appendix E – Data of design 3 at different current densities

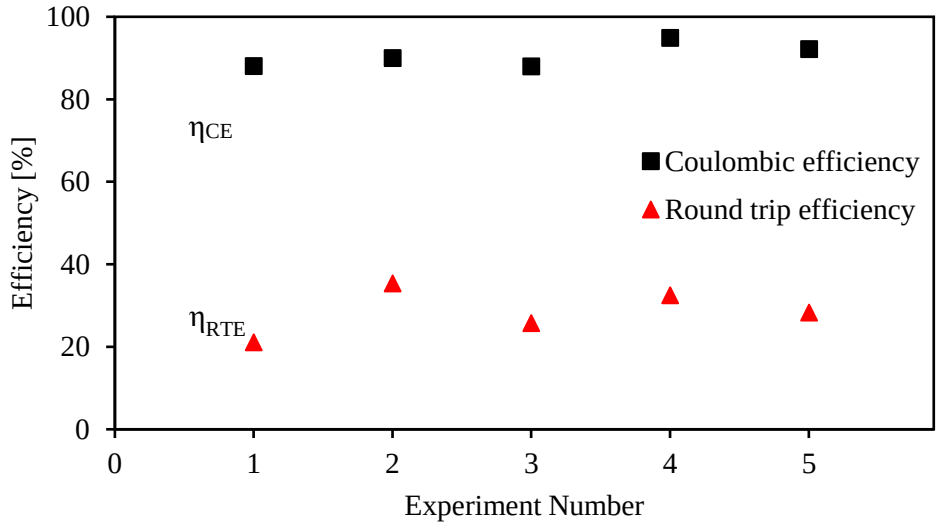

Figure 36 - Coulombic efficiency (η_{CE}) and round-trip efficiency (η_{RTE}). Despite the large compartment thickness of 7 mm a round-trip efficiency of 35.3% was obtained. The highest coulombic efficiency (94.9 %) was reached for current densities of 50 Am^{-2} charging and 37.5 Am^{-2} discharging.

Table 14 - Coulombic efficiency, round-trip efficiency and resistance of design 3 experiments

	CH – DCH A/m^2	Coulombic Efficiency (%)	Round trip efficiency (%)	Resistance [Ωcm^2]	Date
1	100 - 50	88.0	21.1	62.09	29.06
2	37.5 – 37.5	90.0	**35.3**	64.65	21.07
3	50 – 50	88.0	25.7	65.32	25.07
4	50 – 37.5	**94.9**	32.5	68.38	27.07
5	37.5 – 37.5	92.1	28.3	67.71	30.07